Synapse-Specific Modulation of Synaptic Responses by Brain States in Hippocampal Pathways

Manon Rampon, Julien Carponcy, Mégane Missaire, Romain Bouet, Regis Parmentier, Jean-Christophe Comte, Gaël Malleret, Paul Salin

Systems/Circuits

Synapse-Specific Modulation of Synaptic Responses by Brain States in Hippocampal Pathways

Manon Rampon,[1,2*] Julien Carponcy,[1,2,3*] Mégane Missaire,[1,2*] Romain Bouet,[2] Regis Parmentier,[1,2] Jean-Christophe Comte,[1,2] Gael Malleret,[1,2] and Paul A. Salin[1,2]

[1]Forgetting processes and cortical dynamics' team, Centre de Recherche en Neurosciences de Lyon, University Claude Bernard Lyon 1, Bron, F-69500, France, [2]Centre National de la Recherche Scientifique Unité Mixte de Recherche 5292, Institut National de la Santé et de la Recherche Médicale U1028, Bron, F-69500, France, and [3]Medical Research Council Brain Network Dynamics Unit, University of Oxford, Oxford, OX1 3TH, United Kingdom

Synaptic changes play a major role in memory processes. Modulation of synaptic responses by brain states remains, however, poorly understood in hippocampal networks, even in basal conditions. We recorded evoked synaptic responses at five hippocampal pathways in freely moving male rats. We showed that, at the perforant path to dentate gyrus (PP-DG) synapse, responses increase during wakefulness compared with sleep. At the Schaffer collaterals to CA1 (SC-CA1) synapse, responses increase during non-REM sleep (NREM) compared with the other states. During REM sleep (REM), responses decreased at the PP-DG and SC-CA1 synapses compared with NREM, while they increased at the fornix to nucleus accumbens synapse (Fx-NAc) during REM compared with the other states. In contrast, responses at the fornix to medial PFC synapse (Fx-PFC) and at the fornix to amygdala synapse (Fx-Amy) were weakly modulated by vigilance states. Extended sleep periods led to synaptic changes at PP-DG and Fx-Amy synapses but not at the other synapses. Synaptic responses were also linked to local oscillations and were highly correlated between Fx-PFC and Fx-NAc but not between Fx-Amy and these synapses. These results reveal synapse-specific modulations that may contribute to memory consolidation during the sleep–wake cycle.

Key words: **amygdala; local field potential oscillations; medial prefrontal cortex; nucleus accumbens; sleep–wake cycle; dentate gyrus**

Significance Statement

Surprisingly, the cortical network dynamics remains poorly known at the synaptic level. We tested the hypothesis that brain states would modulate synaptic changes in the same way at different cortical connections. To tackle this issue, we implemented an approach to explore the synaptic behavior of five connections upstream and downstream the rat hippocampus. Our study reveals that synaptic responses are modulated in a highly synapse-specific manner by wakefulness and sleep states as well as by local oscillations at these connections. Moreover, we found rapid synaptic changes during wake and sleep transitions as well as synaptic down and upregulations after extended periods of sleep. These synaptic changes are likely related to the mechanisms of sleep-dependent memory consolidation.

Introduction

Mammals continually adapt their behavior to their internal state and surrounding environment. This adaptation is coupled with dynamic brain state changes characterized by rapid shifts in EEG and local field potentials (LFP). The best-defined brain states are those observed during the sleep–wake cycle. Wakefulness is divided into two states in rodents, active wake (AW) and quiet wake (QW) characterized by different motor activities and the presence (AW) or absence (QW) of small-amplitude fast oscillations. In contrast, during sleep, brain states are characterized by high amplitude slow oscillations during non-REM sleep (NREM) and low amplitude fast oscillations during rapid eye movement sleep (REM). Both sleep states contribute to consolidate information that has been encoded during wakefulness (Rasch and Born, 2013).

The memory consolidation is believed to depend on changes in synaptic efficacy in the hippocampal networks. Do vigilance states impact synapses uniformly or, on the contrary, do they selectively modulate the synaptic responses to certain connections? The Synaptic Homeostasis Hypothesis states that synaptic

Received Apr. 19, 2022; revised Dec. 16, 2022; accepted Dec. 19, 2022.

Author contributions: M.R., J.C., M.M., and R.P. performed research; M.R., M.M., and P.A.S. analyzed data; J.C., R.P., and P.A.S. designed research; R.B. and J.C.C. contributed unpublished reagents/analytic tools; G.M. and P.A.S. wrote the paper; P.A.S. wrote the first draft of the paper; J.C. and P.A.S. edited the paper.

This work was supported by Fondation pour la Recherche Médicale to M.R.; Agence nationale de la recherche Depression and Sleep Project to P.A.S. and G.M.; Region Rhone-Alpes to P.A.S.; and Fédération pour la Recherche sur le Cerveau to G.M. We thank researchers, engineers, and students at different stages of the project and especially Vincent Hok, Paul-Antoine Libourel, and Nicolas Fourcaud-Trocme, for the generous help.

*M.R., J.C. and M.M. contributed equally to this work.

The authors declare no competing financial interests.

Correspondence should be addressed to Paul A. Salin at paul.salin@sommeil.univ-lyon1.fr.

https://doi.org/10.1523/JNEUROSCI.0772-22.2022

responses that increase during wakefulness and selectively decrease during NREM that follows wakefulness (Tononi and Cirelli, 2014). Synaptic downscaling has been suggested in the cortex, particularly in the callosal connections of the frontal cortex with electrophysiological methods and in the hippocampus (Hpc) by biochemical methods that do not allow to identify the connections (Vyazovskiy et al., 2008). Conversely, recent studies have suggested that vigilance states had different impact of synaptic responses of neocortical connections (Chauvette et al., 2012; Frank, 2015; Cary and Turrigiano, 2021; Raven et al., 2018; Puentes-Mestril et al., 2019). However, it is within the Hpc that memory mechanisms have been mainly studied. Strangely synaptic changes in hippocampal networks during brain state changes remain poorly described. Synaptic transmission in the Hpc appears differentially gated by vigilance states (Winson and Abzug, 1977). They showed that at the perforant path (PP) to the dentate gyrus (DG) synapse, synaptic responses increase during wakefulness compared with sleep. Later, other studies suggested that synaptic transmission at the Schaffer collaterals (SC) to CA1 pathway decreases during REM compared with NREM and with the occurrence of theta oscillation (Leung, 1980). Thus, a given sleep state may exert opposite modulation of synaptic responses in different hippocampal networks, a result that may have consequences concerning the knowledge we have on the role of brain states in memory processes.

While the PP-DG and SC-CA1 synapses play a critical role in memory, other hippocampal pathways were found to be involved in memory. Among them, connections between the Hpc and the mPFC constitute a major hub for memory consolidation (Maingret et al., 2016). The connections between the Hpc and the NAc have also been involved in forms of memory underlying contextual fear conditioning and appetitive learning (Levita et al., 2002; LeGates et al., 2018; Trouche et al., 2019). The connection between the Hpc and the amygdala (Amy) is also important for encoding a context related to an emotional memory (Zhang et al., 2015). Given the role of the pathways between these areas and the Hpc in memory and the sleep role in these processes, it is surprising that sleep-dependent modulation of synapse has not been studied at these connections.

To better understand the link between brain state dynamics and synaptic changes, we performed long-term recordings of evoked synaptic responses in five different areas: DG, CA1, PFC, NAc, and Amy of freely moving rats. We assessed, within the Hpc, the synaptic transmission at the PP to DG (PP-DG) synapse and at the SC-CA1 synapse, and in three hippocampal outputs between the fornix (Fx), which consists of axons from the Hpc, and the NAc (Fx-NAc synapse), the mPFC (Fx-PFC synapse), and the Amy (Fx-Amy synapse) (Boeijinga et al., 1993). We wanted to find out whether synaptic responses change simultaneously and in the same fashion in these different hippocampal pathways across different brain states, or not.

Materials and Methods

Animals. We used data collected from 40 Dark Agouti male rats (Janvier Labs) at the age of 10-15 weeks and weighing between 200 and 250 g. Animals were maintained in individual cages on a 12 h/12 h light-dark cycle (9:00 A.M. to 9:00 P.M.) at a room temperature of 24°C with food and water *ad libitum*. The animal care and treatment procedures were in accordance with the regulations of the local Lyon 1 University CE2A-UCBL 55) and European Union Council (2010/63/EU) ethics committee for the use of experimental animals. The protocol was approved by the French ethical committee for the use of experimental animals (Permit Number DR2016-29). Efforts were made to minimize the number of animals, or any pain and discomfort occurred to them during surgical or behavioral procedures.

Surgery. Rats were first anesthetized in an induction chamber under isoflurane (2%-2.5%), then placed in a stereotaxic frame where anesthesia was maintained by a 0.75%-1% isoflurane gas mix enriched in oxygen. After incision of the scalp, craniotomies were performed at the position of the electrodes and screws. Reference screws were fixed above the cerebellum. All the electrodes were implanted in the right side of the brain, except for EEG electrodes. The position of LFP and stimulating electrodes is illustrated in Figures 1*B*, 2*A*, 3*A*, 4*A*, and 5*A*. One group of rats ($n = 10$) was implanted with a recording array of 8 electrodes in the DG (A: −3.3 mm, L: 2.4 mm, stereotaxic coordinates are given relative to bregma, in the anteroposterior [A], lateral [L], and depth [D] dimensions; see Fig. 1*B*) (Missaire et al., 2021). The array was lowered ~1 mm below the CA1 stratum pyramidale, which was recognizable by a high rate of spiking activity (D ~ 2.6 mm) until the modest spiking activity of the DG was visualized (D ~ 3.5 mm). The PP stimulating electrode was then lowered (A: −7.5 mm, L: 4 mm) while stimulating at 0.33 Hz and was fixed at the depth corresponding to the expected evoked response (D ~ 3.7 mm). This first group of rats was also implanted with one EEG screw above the PFC and one EEG screw above the parietal cortex on the left side of the brain. Another group of rats ($n = 25$) was implanted with recording electrodes at three different synapses. First, the CA1 electrode was lowered (A: –4 mm, L: 2 mm; see Fig. 2*A*) until visualization of the high spiking activity of the CA1 stratum pyramidale (D ~ 2.5 mm) and fixed 100-200 μm under this layer. We then lowered the SC-stimulating electrode (A: –4 mm, L: 3.1 mm) while stimulating at 0.33 Hz until visualization of the best evoked response in CA1 (D: 3-3.5 mm). Subsequently, we lowered and fixed the recording electrodes in the PFC (A: 2.5 mm, L: 0.5 mm, D: 4 mm), the NAc (A: 1.2 mm, L: 0.8 mm, D: 7 mm), and the Amy (A: −3.2, L: 4.8, D: 8.5). Then, we began the descent of the Fx stimulating electrode (A: −1.7 mm, L: 0.7 mm, D:4.2-4.4 mm) (see Figs. 2*A*, 3*A*, 4*A*, and 5*A*) until we obtained stereotyped responses in the PFC, the NAc, and the Amy as described in several studies (Mulder et al., 1997, 1998). Paired-pulse stimulations were applied with a 50 ms delay to assess paired-pulse depression (PPD) or paired-pulse facilitation (PPF) of the PP-DG, SC-CA1, Fx-PFC, and Fx-NAc synapses. For both groups of rats, two EMG electrodes were implanted bilaterally in the neck muscles. All electrodes were connected to an electrode interface board (EIB-27, Neuralynx) and a protective hat was made with dental cement. At the end of the surgical procedures, a subcutaneous injection of 3 ml of glucose (2.5%) supplemented with carprofen (5 mg/kg) was given to the animals.

Recording conditions. One week after surgery, rats were introduced in their recording chambers and plugged for recording. The recording chambers consisted of a 60 × 60 × 60 cm faradized box with removable container for the litter, so that the rats could be changed daily at 10:00 A.M. without being unplugged. While in the recording chambers, the animals were provided with food and water *ad libitum*. Once the synaptic transmission was stabilized, and after at least 2 d of habituation, recordings took place during several days.

Recording setup. For the group of rats implanted in the DG, the recording array (700 µm × 300 µm) was made of 8 tungsten wires (45 µm diameter) arranged on two lines of 4 electrodes (Missaire et al., 2021). The stimulating electrode lowered in the PP was made of two stainless-steel twisted wires (100 µm in diameter California Fine Wire) deinsulated at the tip. For the second group of rats, the recording electrodes consisted of two twisted tungsten wires (25 μm in diameter California Fine Wire) deinsulated at the tip. Stimulating electrodes were made either with two twisted tungsten wires (45 μm in diameter) or two stainless-steel twisted wires (100 μm in diameter California Fine Wire), also deinsulated at the tip. For both groups of rats, EMG electrodes were made by golden plating a small and round solder ball at the deinsulated and hooked tip of a conventional small electric wire. All these electrodes, along with reference screws, were connected to a custom-made 16 channels analog preamplifier using the EIB-27 connector. The signals were then conveyed via an electric rotary joint (Plastics One) to a 16-channel amplifier (AM-Systems) within which these signals were amplified with a gain of 1000. Signals from the different electrodes were then acquired

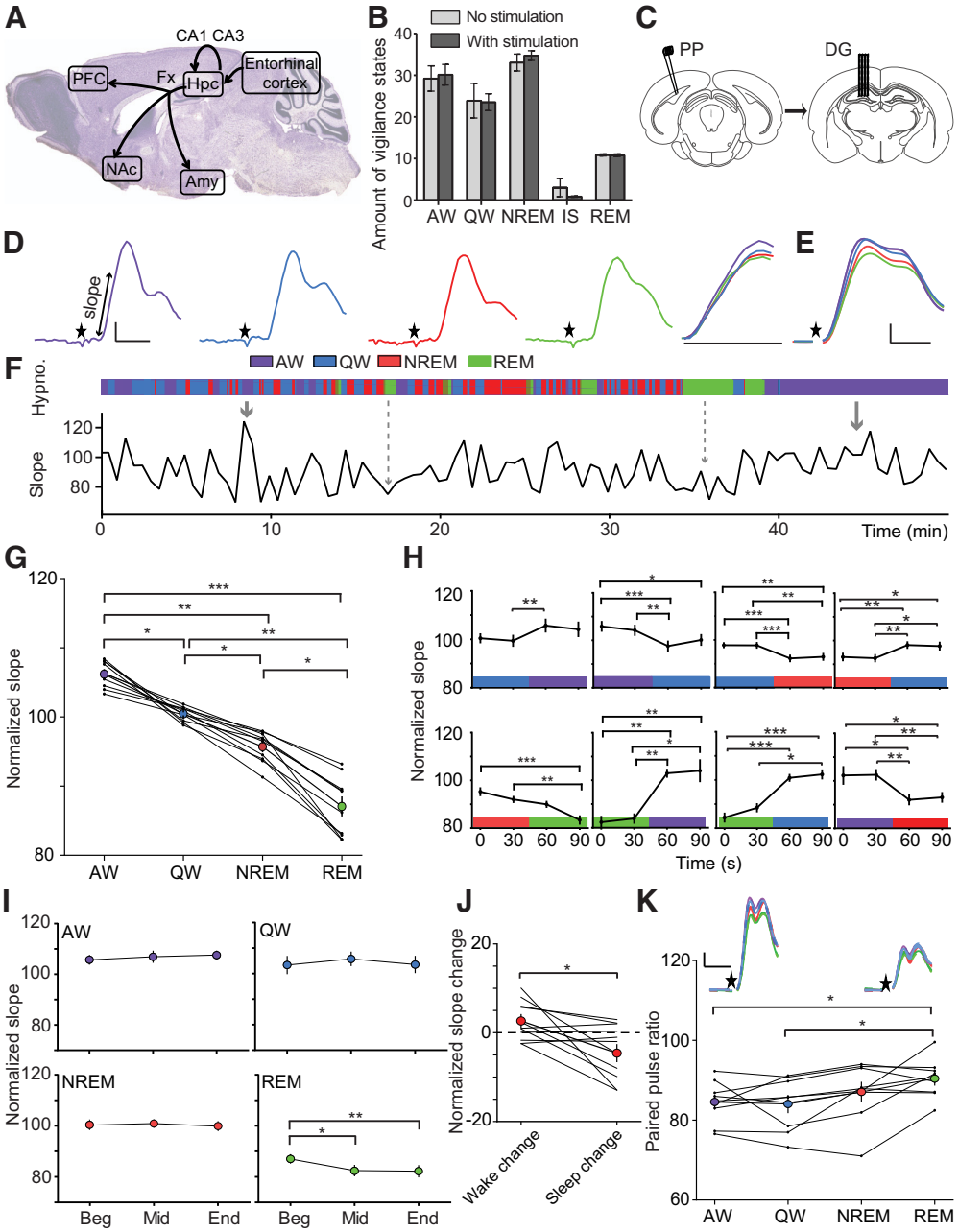

Figure 1. The response at the PP-DG synapse is increased during waking compared with sleep states. ***A***, Sagittal section of the rat brain illustrating the schematic locations of recording and electrical stimulation sites. In one group of rats, synaptic responses were evoked at the PP to the DG synapse; and in another group of rats, the synaptic responses were evoked at the SCs to CA1 area of the dorsal Hpc synapse and at the Fx to the mPFC, the NAc, and the Amy synapses. ***B***, Percentage of vigilance state amount in a group of rats before and after 24 h of electrical stimulation of CA3 area and Fx ($n = 15$). No change in the amount of vigilance states was observed after continuous electrical stimulation (>24 h). ***C***, To evoke responses of the PP-DG synapse, stimulating electrodes were located in the PP (close to the medial entorhinal cortex) and an array of eight recording electrodes were placed in the superior blade of the DG of the dorsal Hpc. ***D***, Typical single fEPSP trace during the four vigilance states. Right, Enlargement of the initial part of the single fEPSPs showing their slopes (superimposed traces). Calibration: 0.2 mV, 2.5 ms. ***E***, Average of all synaptic responses for AW, QW, NREM, and REM during 24 h of continuous recording in the same animal. Calibration: 0.2 mV, 2.5 ms. ***F***, Dynamics of the vigilance states during 1 h of recordings (diurnal period) in the same animal during the same period. Thick arrows indicate increase in synaptic response, observed during AW. Dashed arrows indicate a decrease in synaptic responses, usually observed during REM. Data were normalized to the average of the synaptic slopes obtained during a continuous 24 h period. ***G***, During wakefulness, synaptic responses increased compared with sleep (Friedman test, $\chi^2_{(3)} = 30$, $p = 1.38e^{-06}$, $n = 10$ rats). During REM, synaptic responses drop significantly compared with all other vigilance states. The number of fEPSPs analyzed was 5044 for AW, 4089 for QW, 7595 for NREM, and 2241 for REM. ***H***, The slope of the synaptic responses changed rapidly during transitions between two distinct vigilance states. The normalized slope of synaptic responses was averaged at the four points of each sequence. Synaptic transmission rapidly decreased within 30 s during the transitions AW-QW, QW-NREM, and NREM-REM and increased during the transition REM-AW. Transitions between vigilance states were first selected, and then the synaptic responses were averaged for each rat at the four points of each sequence 30 s apart. Only the most frequent transitions are illustrated (mean ± SEM). ***I***, Intra-episode modulation of synaptic response at the PP-DG synapse. Slope quantification was obtained by subdividing each vigilance state episode in three bouts. During REM, synaptic responses rapidly decreased while synaptic responses were not significantly modulated during the other vigilance state episodes. ***J***, Synaptic changes dependent on prolonged periods of sleep. To quantify the synaptic changes induced by extended periods of sleep, periods with a high density of sleep episodes (>75%) lasting >30 min were selected, and then the synaptic changes were computed in NREM immediately before and after this period. The same quantification was performed with a prolonged period of wakefulness. We performed this quantification over 24 h for each of the synapses of each rat. Black lines connect averaged data from the same rats after an extended period of wakefulness (left) and sleep (right). ***K***, Modulation of PPD during vigilance states. PPD decreased during REM compared with wakefulness. ***$p < 0.001$. **$p < 0.01$. *$p < 0.05$.

and digitized at 5 kHz by a custom MATLAB software (The MathWorks) driving a NI-6343 acquisition board (National Instruments) before being stored on a computer. For all rats, continuous LFP recordings were acquired during a full recording period of several days.

Electrical stimulation. During recording, stimulations consisted of 200 μs monophasic current pulses delivered by an isolated pulse stimulator (model 2100 A.M. Systems). The interval between two stimulations on the same electrode was at least 30 s, and for the second group of rats implanted for recording at three synapses the delay between the two stimulation sites Fx and SC was at least 15 s. During the habituation period, evoked responses were tested by gradually incrementing the current intensities of the electrical stimulations until we obtained clear and typical postsynaptic potentials on at least one pathway. For PP stimulation, the intensity ranged from 140 to 640 µA (mean: 231 µA). For SC, the stimulation intensity ranged from 120 to 300 μA (mean: 202 µA). For Fx, the stimulation intensity ranged from 80 to 600 μA (mean: 291 µA). Stimulus intensities were selected at ~50%-75% of the intensity necessary to evoke the maximum amplitude of fEPSP. To control a potential disturbing effect of electrical stimulation on vigilance states, we compared for each rat the amount of vigilance states during several days of stimulation with a period of the same duration without stimulation. We found that electrical stimulation had no effect on vigilance state amounts (see Fig. 1*B*).

Short-term plasticity evoked by paired-pulse stimulation. Paired-pulse stimulation of synaptic responses at short intervals evoked PPD or PPF of responses at many brain synapses. PPD and PPF represent a form of short-term plasticity. Modulation of the paired-pulse ratio (PPR) of evoked synaptic responses has been shown to depend on presynaptic mechanisms of neurotransmitter release (Stevens and Wang, 1995; Salin et al., 1996). Paired-pulse stimulation of evoked responses was conducted using a 50 ms interstimulus interval from 9:00 A.M. to 5:00 P.M. for each animal. While PPD was observed at PP-DG synapse (Fig. 1*J*), PPF was found at SC-CA1, Fx-PFC, and Fx-NAc synapses (see Figs. 2*I*, 3*I*, and 4*I*). For quantification of the paired-pulse stimulation, we divided the slope of the second stimulation by the first one. We thus obtained a percentage of PPD or PPF for each synapse of each animal in the different vigilance states (see Figs. 1*J*, 2*I*, 3*I*, and 4*I*). A short interstimulus interval (i.e., 50 ms) was chosen to minimize the contribution of the feedback inhibition in the fEPSP evoked by the second stimulation. It is possible, however, that the PPF and PPD are in part a reflection of this inhibitory process.

Histologic verification. At the end of all recordings, electrode locations were marked by passing currents (1 or 3 s, 500 µA) under anesthesia (isoflurane 2%). The brain was then extracted, cryoprotected in a sucrose solution (30%), and frozen. Transverse sections (40 µm) were performed using a cryostat and a neutral red staining was conducted on brain slices. The electrode placements were thus verified and reported on schemes taken from the atlas of Paxinos and Watson (2006).

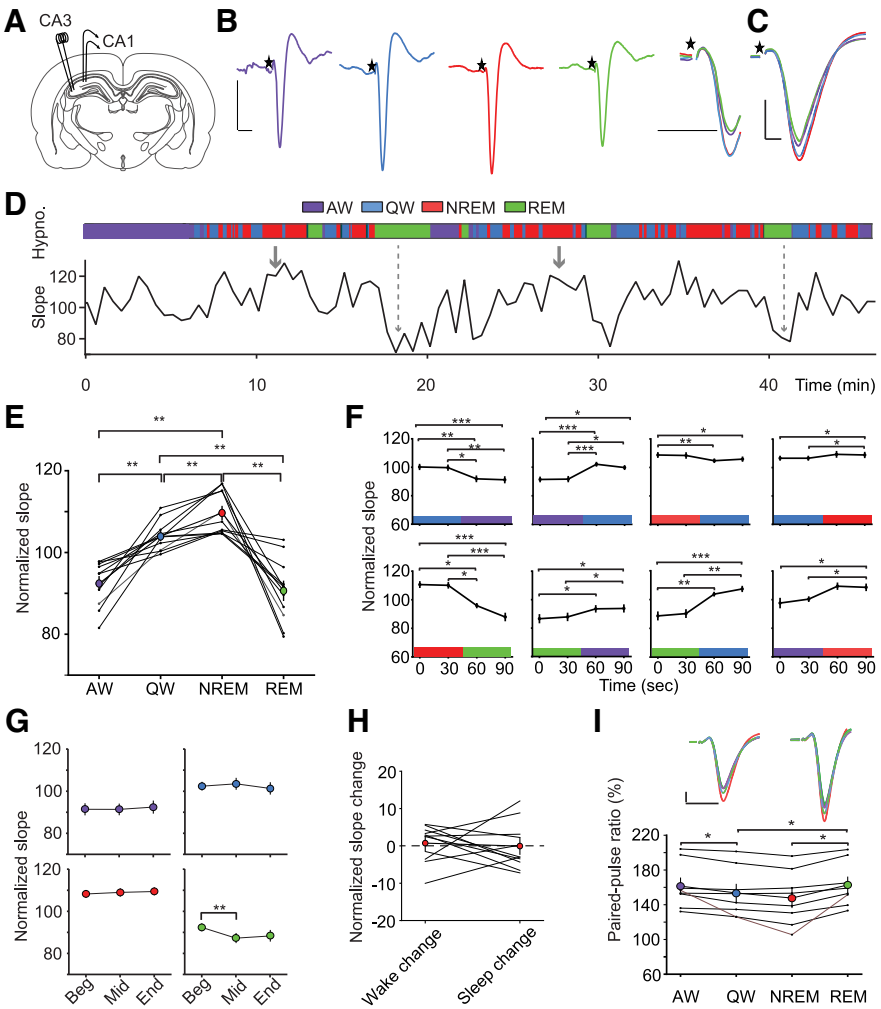

Figure 2. SC-CA1 evoked synaptic responses are increased during NREM sleep and QW compared with AW and REM sleep. ***A***, To evoke responses at the SC-CA1 synapse, two stimulating electrodes and two recording electrodes were placed, respectively, in the stratum radiatum of area CA3 and the stratum radiatum of the CA1 area in the dorsal Hpc. ***B***, Modulation of SC-CA1 synaptic responses during the sleep–wake cycle. Top, Single fEPSP trace during AW, QW, NREM, and REM. Right, Enlargement of the initial part of the single fEPSPs showing their descending slopes (superimposed traces). Calibration: 0.5 mV, 10 ms. Middle, Dynamics of the vigilance states during 1 h of recordings during the diurnal period. ***C***, Average of synaptic responses at SC-CA1 synapse during 24 h. Calibration: 1 mV, 2.5 ms. ***D***, Bottom, Modulation of the normalized synaptic responses in the same animal during the same period. Thick arrows indicate increase in synaptic slope, observed during NREM. Dashed arrows indicate a decrease in synaptic transmission, more specifically observed during REM. ***E***, Each state of vigilance corresponds to a specific modulation of synaptic responses at SC-CA1 synapse. During NREM, synaptic responses were increased compared with the other states, although during REM, synaptic responses decrease significantly compared with all other vigilance states. Large circles represent the average (with SEM) of individual data from each rat (represented by small circles). The number of fEPSPs analyzed was 6987 for AW, 7126 for QW, 9345 for NREM, and 2937 for REM ($n = 11$ rats). ***F***, Synaptic responses changed rapidly during transitions between vigilance states at SC-CA1 synapse. An increase in fEPSP was observed between the transition from AW to QW, the transition from QW to NREM, and the transition from REM to AW. On the other hand, the synaptic response decreased sharply from NREM to REM. ***G***, Intra-episode modulation of synaptic slopes. Slope quantification was obtained by subdividing each vigilance state episode in three bouts. During REM, synaptic responses rapidly decreased. ***H***, Synaptic changes dependent on extended periods of sleep or wakefulness. This quantification was performed over 24 h for each of the synapses of each rat. Black lines connect averaged data from the same rats after an extended period of wakefulness (left) and sleep (right) at the SC-CA1 synapse. ***I***, Modulation of PPF at the SC-CA1 synapse by vigilance states. PPR increased during REM compared with wakefulness. At this synapse, PPR also increased during AW compared with QW and decreased during NREM compared with REM. Calibration: 10 ms, 0.5 mV. ***$p < 0.001$. **$p < 0.01$. *$p < 0.05$.

Vigilance state classification. Offline inspection of EMG, EEG (only for the group of rats implanted at the PP-DG synapse), and/or LFP spectral analysis were used to identify the vigilance states of the animals by bouts of 5 s. We classified them into five categories: two waking states

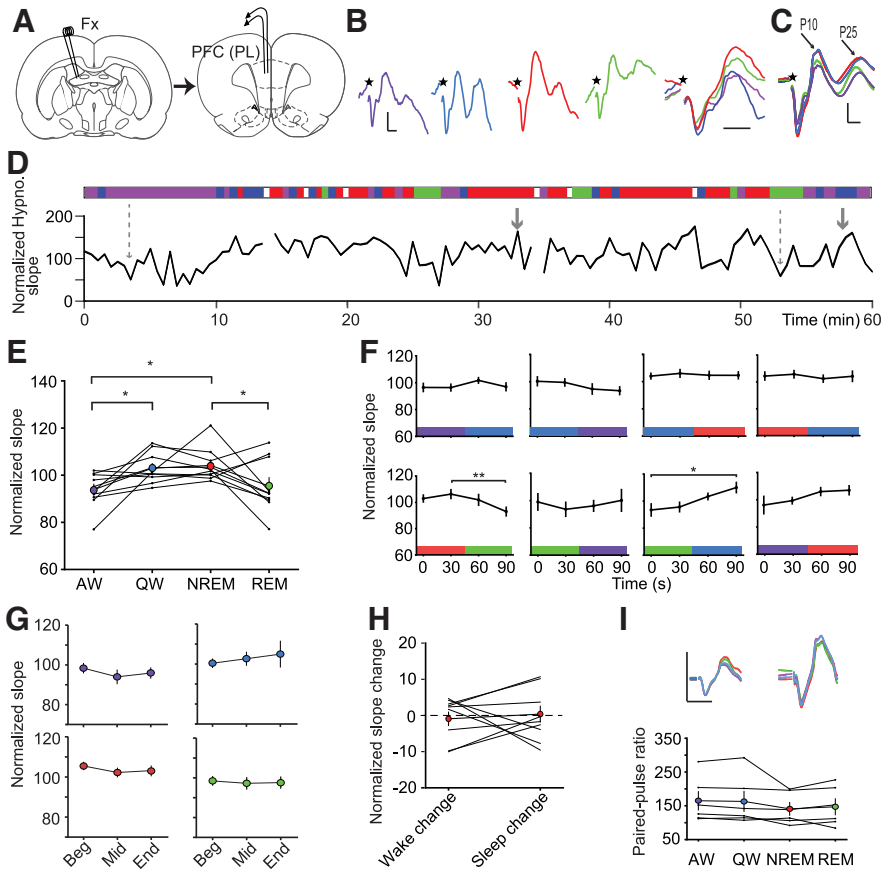

Figure 3. Fx-mPFC evoked synaptic responses are increased during NREM sleep and QW compared with AW and REM sleep. ***A***, To evoke responses at the Fx-PFC synapse, two stimulating electrodes were placed in the Fx and two recording electrodes were placed in the prelimbic area (PL) of the PFC. ***B***, Modulation of Fx-PFC synaptic responses during the sleep–wake cycle. Top, Single fEPSP trace during AW, QW, NREM, and REM. Right, Enlargement of the initial part of the single fEPSPs showing their descending slopes (superimposed traces). ***C***, Average of Fx-PFC synaptic responses during 24 h. Arrow indicates the synaptic response (P10 positive response at 10 ms). Calibration: 0.2 mV, 5 ms. ***D***, Dynamics of the vigilance states during 1 h of diurnal period. Bottom, The time course of synaptic responses in the same animal during the same period. Thick arrows indicate an increase in synaptic response in QW and NREM and a decrease in AW and REM. ***E***, At the Fx-PFC synapse, responses during NREM were increased compared with AW and REM. Responses at this synapse were also increased during QW compared with AW ($n = 9$ rats). ***F***, At the Fx-PFC synapse, a decrease in evoked responses was observed during transition between NREM and REM. For each transition between states represented, the slope of the fEPSP was computed for the two last responses of a given state, and for the two first responses of the following state for each animal. ***G***, Intra-episode modulation of synaptic slopes. No modulation of synaptic slope is observed during REM. ***H***, Synaptic changes dependent on extended periods of sleep or wakefulness. No modulation of the synaptic slope is observed during extended periods of wakefulness or sleep. ***I***, No modulation of PPF by vigilance states was observed at the Fx-PFC synapse. ***$p < 0.001$.

(QW and AW) and three sleeping states (NREM, intermediate sleep [IS], and REM). IS was not included in either NREM or REM because it corresponds to a very different brain state (Gervasoni et al., 2004). AW was recognizable by a theta rhythm in CA1, DG, and EEG signals, and an important muscular activity on EMG. QW was characterized by a weak muscular activity and δ-like activity in the PFC, NAc, and EEG recordings. NREM was characterized by the occurrence of slow waves in PFC, NAc, and EEG signals and a very weak muscle activity. REM was determined by a prominent theta rhythm in CA1, DG, and EEG recordings and muscle atonia on EMG (Fig. 6). IS, located between NREM and REM, was characterized by a combination of slow waves and theta rhythm in PFC and EEG recordings, along with muscle tone declining toward atonia. Because of the very short duration of IS, and thus the very small number of synaptic responses collected during that state, we choose not to analyze it. Recording periods that did not fulfill the criteria for vigilance states (because of movement artifacts or drowsiness between wakefulness and NREM) were discarded. The percentage of recording time eliminated from the analyses (because of artifacts in the EEG, LFP, and EMG signals, drowsiness and SI periods) was in average 7.03 ± 0.9% ($n = 33$ rats).

Synaptic responses. Figures 1*B*, 2*A*, 3*A*, 4*A*, and 5*A* show a schematic of the position of recording and stimulating electrodes used to study the five synapses of interest linked to the hippocampal circuit. Animals were only included in the dataset after histologic verifications of the electrode sites. Several animals were thus discarded from the database, at the PP-DG synapse (5 of 15 rats), the CA3-CA1 synapse (5 of 18 rats), the Fx-PFC synapse (7 of 18 rats), the Fx-NAc synapse (7 of 18 rats), and the Fx-Amy synapse (6 of 16).

At the PP-DG synapse, animals displayed a clear positive (excitatory) peak with a delay of 3.5-5.5 ms after the stimulus artifact in at least 1 of the 8 electrodes of the recording array. The positive polarity of the fEPSPs recorded at this synapse (Fig. 1*C*,*D*) corresponds to the depolarizing responses of the intracellular synaptic potentials generated at this synapse (Colino and Malenka, 1993). For the slope analysis of these fEPSP-evoked potentials, data were averaged on all electrodes displaying a clear positive peak with a linear slope. In average per animal, during 24 h, we analyzed the following number of fEPSPs: during AW = 627 ± 48, during QW = 479 ± 26, during NREM = 792 ± 35, during REM = 252 ± 16, $n = 10$ rats.

At the SC-CA1 synapse, evoked responses presented one clear excitatory negative peak with a delay of 5-10 ms after electrical stimulation. The negative polarity of the fEPSP recorded at this synapse (Fig. 2*B*,*C*) corresponds to the depolarizing responses of the intracellular synaptic potentials generated at the SC-CA1 synapse (Andersen et al., 1980). In average, during 24 h, we analyzed the following number of fEPSPs by rats: AW = 635 ± 75, QW = 648 ± 51, NREM = 850 ± 31, REM = 277 ± 23, $n = 11$ rats.

Stimulation of the Fx evoked a monosynaptic response in the three efferent structures (PFC, NAc, and Amy). For the PFC, the majority of recording sites were located in the prelimbic area; for the NAc, the recording sites were located in the shell; and for the Amy, the recording sites were located in the basolateral area. The Fx connections are constituted by axons of the ventral Hpc and also the dorsal CA1 Hpc (Trouche et al., 2019). Evoked LFP responses at the Fx-PFC, Fx-NAc, and Fx-Amy synapses were analyzed when these responses presented the three following criteria: an early negative deflection of ~5 ms after stimulation called N5, and two positive peaks at ~9 ms and 23 ms after stimulation referred as P10 and P25 (Figs. 3*B*,*C*, 4*B*,*C*, and 5*B*,*C*). The positive polarity of the fEPSP at Fx-NAc synapse (the monosynaptic P10 component, Fig. 4*B*,*C*) corresponds to the depolarizing responses of the intracellular synaptic potentials generated at the Fx-NAc synapse (Boeijinga et al., 1993; Mulder et al., 1997; Mulder et al., 1998). The Fx-NAc synapse we recorded here mainly corresponds to the connections of the pyramidal cells of the ventral Hpc to the dopamine D1 receptor-expressing medium spiny neurons in the medial NAc shell, although a contribution of pyramidal cell axons from the dorsal Hpc to fast-spiking interneurons in the NAc is also present (Trouche et al., 2019). At the Fx-NAc synapse, data from 11 animals were conserved and responses were analyzed during a 24 h period. A total of 4882 responses were thus collected during AW, 4374 during QW, 7210 during NREM, and 2089 during REM (means by rats: AW = 444 ± 73, QW = 398 ± 64,

NREM = 655 ± 94, REM = 190 ± 32). For the Fx-PFC synapse, the dataset was constituted of 9 animals (mean ± SEM by rats: AW = 539 ± 80, QW = 469 ± 38, NREM = 823 ± 45, REM = 242 ± 11). Evoked LFP responses at the Fx-Amy synapse (10 rats) were analyzed when these responses presented the three following criteria: an early negative deflection of ~5 ms after stimulation called N5, and two positive peaks at ~9 ms and 23 ms after stimulation referred as P10 and P25 (Fig. 5*B*,*C*). For the quantification of the evoked response at this synapse, we computed the positive slope of the component P10. The shape of evoked responses we obtained at this synapse was very similar to the one observed in anesthetized rats (Mulder et al., 1998). The evoked responses recorded at synapses downstream the Hpc (Fx-NAc, Fx-PFC, and Fx-Amy synapses) mainly reflect synaptic responses (Boeijinga et al., 1993). However, as with other evoked synaptic responses recorded in LFP, we cannot eliminate a contribution from feedforward inhibition, population spike, and active conductance mixed with the excitatory synaptic response. To minimize such a contribution, we preferred the measurement of the slope to the measurement of the peak amplitude of the response. Slope measurement is also less subject to amplitude variations because of baseline LFP oscillations.

Slope measurement of evoked responses. fEPSPs of 24 h continuous recording were extracted and analyzed offline for slope measurements. The data collected for all animals and in all areas corresponded to the same circadian periods of 24 h: a diurnal (light) phase of 12 h (9:00 AM to 9:00 PM) followed by a nocturnal (dark) phase of 12 h (9:00 PM to 9:00 AM). The stability of the shape and the amplitude of the evoked responses recorded over 24 h were verified by superimposing averaged fEPSP obtained during 3 h recordings (i.e., 8 superimposed averaged traces). Animals with unstable recordings have been removed from the database. The recording instability was most often a progressive decrease or increase in the slope and amplitude of the synaptic response over the eight 3-h period averages of fEPSPs. These progressive changes were also accompanied by a change in the shape of the fEPSPs suggestive of movement of an electrode or a lesion around it. The number of animals removed from the database for recording instability was found at the SC-CA1 (2 of 13 rats) synapse and at the Fx-PFC synapse (2 of 11 rats). Time cursors for fEPSP slope analysis were positioned manually on averaged fEPSP. The slope was computed at the initial part of fEPSP response (between 20% and 50%) for PP-DG, SC-CA1 synapses and between 20% and 80% for Fx-NAc, Fx-PFC, and Fx-Amy synapses. The slope of the fEPSPs was then normalized by dividing their value by the average of the slopes of fEPSPs recorded over 24 h.

Modulation of synaptic responses during transitions between vigilance states. In order to study the time course of synaptic changes during transitions between vigilance states, we averaged the two last fEPSPs (slope) evoked during the episode of a given state (corresponding to a period of 30s, the interval between two stimulations), and the two first fEPSPs evoked during the following state. We thus obtained four time points for each transition between vigilance states, and the differences of the fEPSP slope between these points were tested by a Friedman ANOVA test. The differences between these different segments were then further assessed by a *post hoc* Dunn's multiple comparison test. Epochs with wakefulness transitions to drowsiness and with NREM transition to IS were removed from the transition analysis.

Modulation of synaptic responses within vigilance state episodes. To assess the dynamic modulation of evoked responses within the different episodes of wakefulness, NREM, and REM, we selected "long duration" episodes (i.e., episodes lasting at least 100 s). We subdivided these datasets into first, middle, and last third of the episodes.

Synaptic changes dependent on prolonged periods of sleep. To quantify the synaptic changes potentially induced by extended periods of sleep or wakefulness (Tononi and Cirelli, 2014; Frank, 2015), we used the "sandwich" method conducted by Cary and Turrigiano (2021). Briefly, this method consists of identifying periods with a high density of

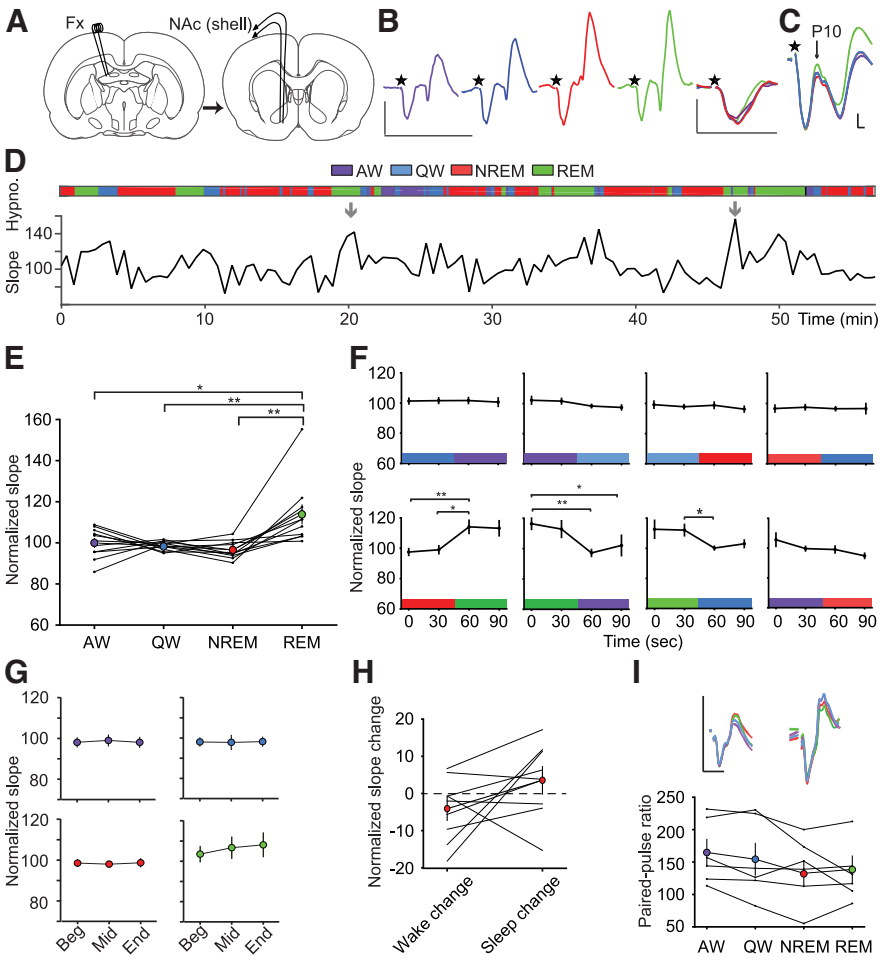

Figure 4. Responses at the Fx-NAc and Fx-Amy synapses were modulated during the sleep–wake cycle. ***A***, To evoke responses at the Fx-NAc synapse, two stimulating electrodes were placed in the Fx and two recording electrodes were placed in the shell of the NAc. ***B***, Top, Single Fx-NAc synaptic response trace during AW, QW, NREM, and REM. Arrows indicate the P10 and P25 evoked responses (positive responses, respectively, at 10 and 20-30 ms). Right, Enlargement of the initial part of the single fEPSPs showing their slopes (superimposed traces). Middle, Dynamics of the vigilance states during 1 h of recordings during the diurnal period. Bottom, The time course of synaptic responses in the same animal during the same period. Thick arrows indicate an increase in synaptic response during REM. Data were normalized to the average of the slope of the synaptic response obtained during a continuous 24 h period. ***C***, Average of the Fx-NAc synaptic responses during 24 h (same animal as in ***A***). ***D***, Modulation of the normalized synaptic responses in the same animal. Thick arrows indicate an increase in synaptic slope during REM compared to the other vigilance states. ***E***, The Fx-NAc synaptic responses were increased during REM compared with wakefulness and NREM ($n = 11$ rats). ***F***, Responses changed rapidly during transitions between vigilance states at the Fx-NAc synapse. A rapid increase in fEPSP slope was observed during transitions between NREM and REM, although a decrease was found at the transition between REM and AW. ***G***, Intra-episode modulation of synaptic slopes. No modulation of synaptic slope is observed during REM. ***H***, Synaptic changes dependent on extended periods of sleep or wakefulness. No modulation of the synaptic slope is observed during extended periods of wakefulness or sleep. ***I***, Modulation of PPF by vigilance states. At this synapse, PPR was not modulated. $^{**}p < 0.01$. $^{*}p < 0.05$.

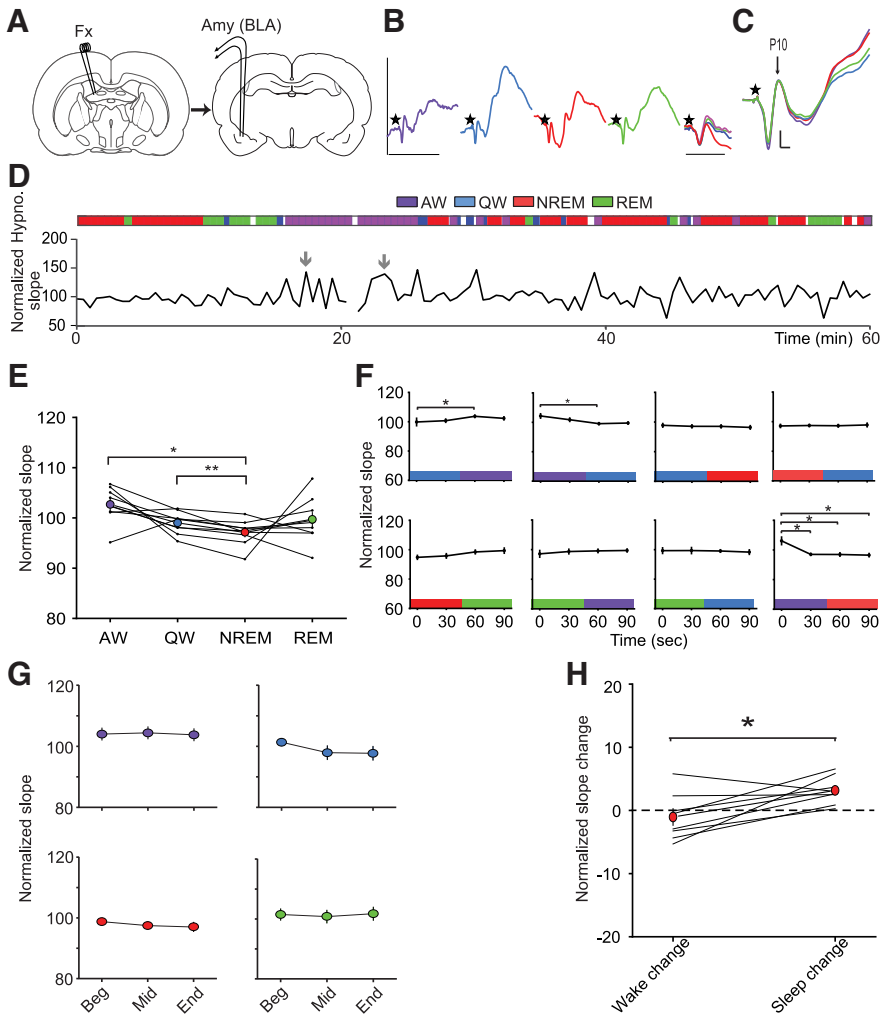

Figure 5. Responses at the Fx-Amy synapses were modulated during the sleep–wake cycle. ***A***, To evoke responses at the Fx-Amy synapse, two stimulating electrodes were placed in the Fx and two recording electrodes were placed in the basolateral Amy. ***B***, The slopes of synaptic responses tend to increase during AW. Top, Single Fx-Amy synaptic response trace during AW, QW, NREM, and REM. Arrows indicate the P10 and P25 evoked responses (positive responses, respectively, at 10 and 20-30 ms). Right, Enlargement of the initial part of the single fEPSPs showing their slopes (superimposed traces). Calibration: 0.2 mV, 5 ms. ***C***, Average of the Fx-Amy synaptic responses. Arrow indicates the P10 synaptic response. ***D***, Dynamics of the vigilance states during 1 h of recordings during the diurnal period. Bottom, The time course of synaptic responses in the same animal during the same period. Thick arrows indicate frequent increases in synaptic response during AW. ***E***, The Fx-Amy synaptic responses were increased during wakefulness compared with NREM ($n = 9$ rats). ***F***, Modulation of synaptic responses at the Fx-Amy synapse during transitions between vigilance states. A decrease in synaptic slope was observed during transitions between AW and QW. Transitions between vigilance states were first selected, and then the synaptic responses were averaged at the four points of each sequence for each animal. ***G***, Intra-episode modulation of synaptic slopes. Slope quantification was obtained by subdividing each vigilance state episode in three bouts. No modulation of synaptic slopes was observed. ***H***, Synaptic changes dependent on extended periods of sleep or wakefulness. A small but significant increase in synaptic slope is observed after extended periods of sleep compared with extended periods of wakefulness. $^{**}p < 0.01$. $^{*}p < 0.05$.

sleep episodes (>75%) lasting >30 min to evaluate the synaptic changes (in NREM) before and after this sleep period. The same quantification was performed with a prolonged period of wakefulness (>30 min) to assess synaptic changes before and after this wake period. We performed this quantification over 24 h for each of the synapses of each rat for comparison of synaptic changes between extended sleep and wake periods.

Analyses of prestimulus LFP recordings. Ongoing LFPs were first recorded in the DG, CA1, PFC, NAc, and Amy simultaneously with the synaptic responses. The correlation between the LFP oscillations immediately preceding the electrical stimulation (1-2 ms delay) and the slope of evoked fEPSPs was then analyzed for each synapse of interest. The following oscillation bands have been selected: slow waves (0.5-2 Hz), δ (2-4 Hz), theta (5-8 Hz), σ (9-14 Hz), low γ (38-45 Hz), and high γ (55-95 Hz). The ripples frequency band (140-220 Hz) was not selected because the position of the recording electrodes in the CA1 area was located in the stratum radiatum and not in the stratum pyramidale to eliminate the presence of population spikes in the fEPSP of the SC-CA1 synapse. We next band pass filtered the LFP signals obtained in the bands of interest (forward and reverse filtering). Measurement of the power of the filtered LFP was then conducted over a prestimulus period of 2 s for slow waves, 1 s for δ oscillations, 500 ms for theta and σ oscillations, and 250 ms for low and high γ oscillations (custom-written MATLAB scripts (The MathWorks). The calculation of the instantaneous oscillation phase was obtained by the argument of the complex analytical signal of the Hilbert transform, and the frequency was obtained by the calculus of the derivative of the instantaneous phase divided by 2π. The amplitude of the oscillations was calculated by the modulus of the analytical signal of the Hilbert transform.

In addition, LFP power spectra were computed for every 5 s epoch within the 0-100 Hz frequency range using a Fourier transform analysis. These spectral analyses were performed using the Chronux toolbox (Chronux data analysis platform from http://chronux.org). To normalize data, power spectral densities were averaged for each frequency range on a 24 h period and each vigilance state. Data were then normalized to the total power (sum of power spectral densities on the 0-100 Hz range on a 24 h period with all vigilance states).

Statistical analysis. All statistical analyses were performed using R (R Core Team, 2021). Figures were created using "ggplot2" R package. For the Friedman tests, the effect size was estimated by computing Kendall W effect size using the "rstatix" package. The effect size (to compare means) is considered large when it is >0.8, medium when it is >0.5, and small when it is <0.5. Given the multiple sources of variability (animal, position of electrodes) and the heteroscedasticity of the variables quantifying oscillations (oscillation power), the statistical analyses of the Figure 4 were conducted using linear mixed-effect models. Mixed-effect models incorporate both fixed-effect parameters and random effects. Lmer of "lme4" package provides tools to analyze mixed effects of linear models (Bates et al., 2015). In contrast with classical regression assuming observations are independent of each other, linear mixed-effect model can account for repeated measurements by estimating random effects in addition to fixed effects for the entire dataset. We analyzed the influence of four possible fixed effects on the slope of evoked responses: (1) four vigilance states as factor; (2) power of frequency bands as numeric; (3) six frequency bands (slow waves: 0.5-2 Hz, δ: 2-4 Hz, theta: 5-8 Hz, σ: 9-14 Hz, low γ: 38-45 Hz; high γ: 55-95 Hz) as factor (see paragraph above); and (4) time of recording (on 24 h). Type II analysis of variance Wald χ^2 tests were used to assess the significance of each fixed effect to the model. For classical linear correlation, the coefficient of determination R^2 allows to estimate the predictive capacity of the model. The total variance in y (synaptic slopes) is explained by all the predictors in the model. However, this coefficient favors the most complex models.

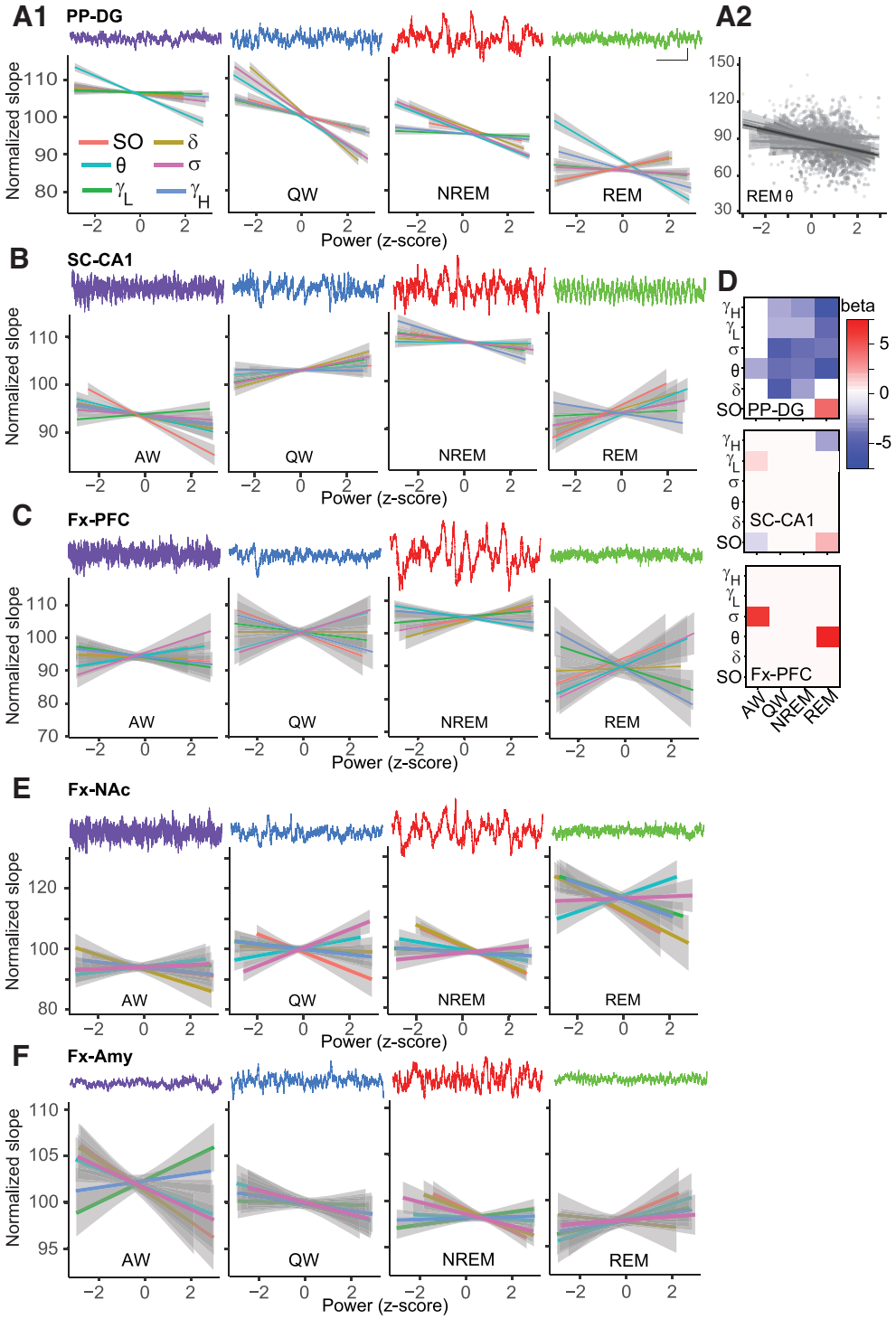

Figure 6. Correlation between the synaptic responses and the magnitude of prestimulus oscillations. ***A***, Correlations between prestimulus oscillation power and synaptic slope at the PP-DG synapse during the sleep–wake cycle (left to right, AW, QW, NREM, and REM). Top, Traces of LFP in the different vigilance states showing δ oscillations during NREM and theta oscillations during AW and REM. Calibration: 100 μV, 1 s. ***A1***, Color code represents the correlations between the different frequency bands (SO, slow waves: 0.5-2 Hz, δ: 2-4 Hz, θ: 5-8 Hz, σ: 9-14 Hz, γL [low γ]: 38-45 Hz; γH [high γ]: 55-95 Hz) and the synaptic slope. Measurement of the power of the filtered LFP was conducted over a prestimulus period of 2 s for slow wave, 1 s for δ oscillations, 500 ms for theta and σ, and 250 ms for low and high γ oscillations. The different regression lines (lm function of *R*, gray lines) indicate the correlation (linear fitting curve and CI) obtained for each rat (24 h recordings). At the PP-DG synapse, during AW, synaptic slopes were negatively correlated with the magnitude of theta oscillations (R^2m = 0.042, $p = 1.23e^{-06}$; β estimate (β): normalized synaptic slope (%)/oscillation power, $\beta = -2.35$; $n = 10$ rats). During QW as well, fEPSPs were negatively correlated with theta oscillations, but also with δ, σ, and γ oscillations (R^2m = 0.093, $p = 6.16e^{-14}$; for δ: $\beta = -5.28$, theta: $\beta = -4.12$, σ: $\beta = -5.06$, low γ: $\beta = -2.93$, high γ: $\beta = -2.98$) as for NREM (R^2m = 0.087, $p = 3.02e^{-12}$, δ: $\beta = -2.62$, theta: −3.91, σ: $\beta = -3.86$, low γ: $\beta = -1.91$, high γ: $\beta = -2.82$). In contrast, during REM, fEPSP slopes were positively correlated with the slow oscillations, although negatively correlated with theta, σ, and γ oscillations (R^2m = 0.073, $p = 2.38e^{-14}$, SO: $\beta = 3.97$, theta: $\beta = -5.35$, σ: $\beta = -3.27$, low γ: $\beta = -3.89$, high γ: $\beta = -5.35$). ***A2***, Detailed observation of ***A1***: the correlation between synaptic slopes at the PP-DG and the magnitude of theta during REM. The different gray regression lines indicate the results obtained for each animal. Black regression line indicates the regression line obtained for the entire dataset. The correlation was negative for all rats. ***B***, At the SC-CA1 synapse, during AW, synaptic slopes were positively correlated with the slow oscillations, although negatively correlated with the low γ oscillations (R^2m = 0.031, $p = 0.0047$, for SO: $\beta = -1.01$ and for low

In order to select the best model, an information criterion approach is preferred, since Akaike information criterion (AIC) and Bayesian information criterion (BIC) indicators penalize for the number of predictors. Thus, AIC and BIC tests were performed to test model fit before and after sequential addition of random effects. After performing these tests, subjects were considered as random effects (for intercept and slope) in all statistical analyses. The fixed effects represent the mean effect across all animals after removal variability (i.e., model: lmer (Dependent Variable (synaptic slopes) ~ 1 + Independent Fixed Effects + (1|animals), data)). To optimize our model, we checked the normality of the model residual. To assess the relationship between the oscillation power and synaptic slopes we computed the β estimates of the regression curves. β, the slopes of predictors, assess the relative contribution of each predictor (oscillation power at a given frequency band) to the overall prediction of the dependent variable (synaptic response quantified by synaptic slopes). The higher the betas are in absolute value, the stronger the link between synaptic responses and oscillations. Beta zero ($\beta 0$), the intercept of the regression curves, corresponds to the average synaptic slope during the different vigilance states. To compare between the different datasets shown in Figure 6, we also computed marginal (R^2m, the proportion of variance explained by fixed effect factors) and conditional coefficients of determination (R^2c, the proportion of variance explained by fixed and random effect factors) (Nakagawa and Schielzeth, 2013). For clarity reasons, only the marginal coefficient of determination (R^2m) is mentioned in Results. For Pearson correlation and partial correlation measurements, the package "correlation" was used. Partial correlations are a measure of the correlation between two variables that remains after controlling for all the other relationships. Fisher z transformation was used to normalize the Pearson correlation coefficients. This explains why in Figure 11*C* the correlation coefficient values can be >1. To detect nonlinearity between the phase of prestimulus LFP oscillations and synaptic responses (see Figs. 7-9), surrogates are obtained by randomizing the data using R. In this figure, the fitting curves and the coefficients of determination of the correlations were conducted using OriginPro software.

Data availability. Data are available via reasonable requests to the corresponding author.

Results

Synaptic responses at the PP-DG, SC-CA1, Fx-NAc, Fx-PFC, and Fx-Amy pathways were monitored during long-term recording in freely moving rats to fully depict the modulation of evoked responses during brain state changes. We first described the behavior of each synapse throughout the sleep–wake cycle.

Vigilance state-dependent modulation of evoked responses at the PP-DG synapse

As shown in a representative sample of 1 h recording (Fig. 1*F*), the slope of the fEPSP at the PP-DG synapse was dynamically modulated during vigilance states. Increases in synaptic response were thus observed during AW episodes (indicated by full line arrows), whereas drops in synaptic amplitude were found during REM episodes (indicated by dashed line arrows). When averaged on a 24 h period of continuous recording, the PP-DG fEPSP waveforms taken from the same animal clearly showed different amplitudes of the synaptic responses during wakefulness and sleep (Fig. 1*E*). The analysis from the entire group of 10 rats indicated a variation of fEPSP slopes at the PP-DG synapse in the following direction: AW > QW > NREM > REM (Fig. 1*G*; Friedman test, $\chi^2_{(3)} = 30$, $p = 1.38\text{e-}06$; *post hoc* Dunn's test $p = 0.01$ between AW and QW, QW and NREM, and NREM and REM; $p = 0.002$ between AW and NREM and QW and REM; $p = 0.001$ between AW and REM; Kendall's effect size = 0.89).

Given the vigilance state-dependent changes at the PP-DG synapse, we then determined the time course of these synaptic changes during transitions between two different consecutive vigilance states. For each transition between wake and sleep states, we observed a significant modulation of synaptic responses (Fig. 1*H*). Large and rapid increase in the synaptic responses of 22% was thus observed during transitions from REM to AW between two consecutive synaptic responses (i.e., 30 s interstimulus interval, Friedman test $\chi^2_{(3)} = 19.7$, $p = 1.98\text{e}^{-04}$). Moreover, synaptic responses were rapidly modulated within 30 s between AW and QW (Friedman test $\chi^2_{(3)} = 20.6$, $p = 1.25\text{e}^{-04}$). Fast changes in synaptic responses were also found for other state transitions (from NREM to REM: a 12% decrease, Friedman test $\chi^2_{(3)} = 23.9$, $p = 2.65\text{e}^{-05}$). We next examined changes in synaptic responses within each vigilance state episodes (Fig. 1*I*). To do so, we computed the evolution of the synaptic responses across the course of the different episodes of AW, QW, NREM, and REM by dividing each episode by thirds (see Materials and Methods). fEPSPs were not modulated during AW ($p = 0.078$), QW ($p = 0.521$), or NREM ($p = 0.436$) episodes. In marked contrast, the synaptic slopes deeply decreased during the course of REM episodes (Friedman test, $\chi^2_{(2)} = 13.9$, $p = 0.0008$), from the beginning to the middle ($p = 0.021$) and from the middle to the last part of the episode ($p = 0.002$), suggesting that synaptic responses were actively modulated during this sleep state.

In order to determine whether sleep induced gradual downregulation (as predicted by Synaptic Homeostasis Hypothesis) or upregulation of synaptic responses, we looked for extended periods of sleep and wakefulness (>30 min, see Materials and Methods) and then compared synaptic responses before and after these periods (Vyazovskiy et al., 2008; Chauvette et al., 2012; Cary and Turrigiano, 2021). Figure 1*J* shows that an extended period of sleep decreased the slope of synaptic responses compared with an extended period of wakefulness ($p = 0.019$, Wilcoxon Signed Rank test, $n = 10$ rats).

We next examined whether a form of short-term plasticity evoked by paired-pulse stimulation was modulated during the sleep–wake cycle (see Materials and Methods). Modulation of the PPR of evoked responses is a form of short-term plasticity that has been shown to depend on presynaptic mechanisms of neurotransmitter release (Manabe et al., 1993; Stevens and Wang, 1995). A decrease in synaptic responses associated with an increase in PPR suggests that neurotransmitter release probability decreased (because of an increased failure rate in the response to the first stimulation of the pair). Reciprocally, an increase in synaptic responses associated with a decrease in PPR strongly suggests that neurotransmitter release probability increases (because of a decrease in the failure rate to respond to the first stimulation). Paired-pulse stimulation at 50 ms interstimulus interval evoked PPD at PP-DG synapse (Fig. 1*K*) as already known (Colino and Malenka, 1993). Here,

←

γ: β =1.204; $n = 10$ rats). In contrast, during REM, fEPSPs were positively correlated with the slow oscillations, although negatively correlated with high γ oscillations (R^2m = 0.008, $p = 0.010$, for SO: β = 2.204 and for high γ: β = −2.53). ***C***, At the Fx-PFC synapse, during AW, we found a positive correlation with σ (R^2m = 0.005 and $p = 0.0048$, for σ: β = 6.25; $n = 9$ rats) and, during REM, a positive correlation with theta (R^2m = 0.019 and $p = 0.003$; for theta: β = 7.07). ***D***, Matrix representing the β parameters of the significant correlations between the synaptic slopes and the power of the different frequency bands for the three cortical synapses. Estimates in blue are negative, whereas estimates in red are positive. The intensity of the color scale indicates the level of the β estimates. ***E***, At the Fx-NAc synapse, no correlation was found in AW (R^2m = 0.001, $p = 0.8$; 9 rats), QW (R^2m = 0.003, $p = 0.8$), NREM (R^2m = 0.001, $p = 0.1$), and REM (R^2m = 0.009 and $p = 0.4$). ***F***, No significant correlation was also found at the Fx-Amy synapse in AW (R^2m = 0.002, $p = 0.051$; 9 rats), QW (R^2m = 0.002, $p = 0.9$), NREM (R^2m = 0.007, $p = 0.06$), and REM (R^2m = 0.002 and $p = 0.9$).

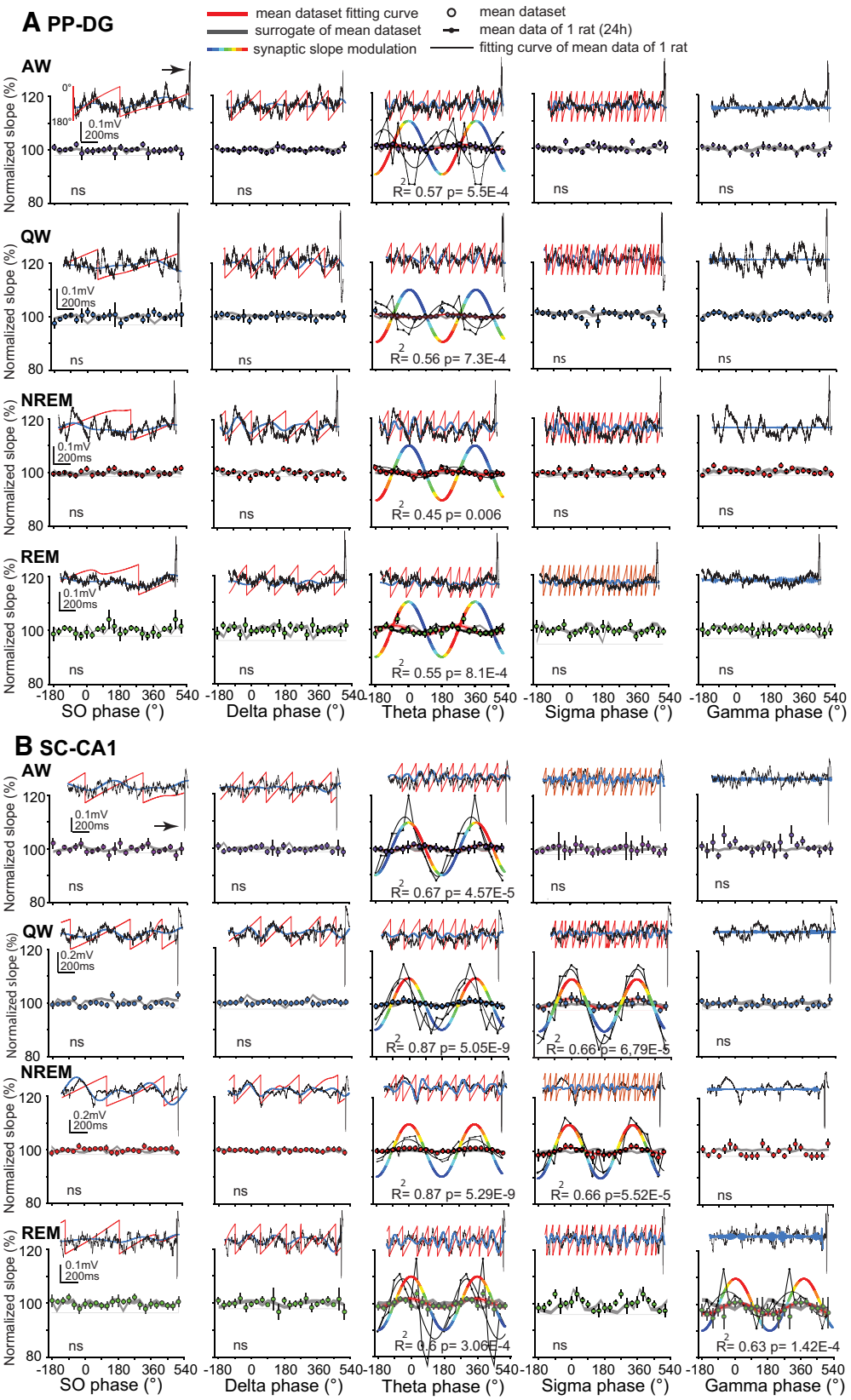

Figure 7. Correlation between the phase of LFP oscillations and the synaptic changes at the PP-DG and SC-CA1 synapses. ***A***, At the PP-DG synapse, correlation between the synaptic slope and the phase of LFP oscillations during AW (purple), QW (blue), NREM sleep (red), and REM sleep (green). Top, Superimposed single traces represent the raw data (black), the filtered data in the waveband (blue). Red represents the phase of the oscillations, except for that of the γ, which does not allow to see these oscillations. Horizontal black arrow indicates the evoked synaptic response. Bottom, Superimposed correlations (gray dots) between the phase (from −180° to 540°) and the synaptic slopes of the database over 24 h. On the same graphs, average correlation of the entire dataset ($n = 10$ rats; purple dots for AW, blue dots for QW, red dots for NREM, and green dots for REM) and the superimposed fitting curve (red with 95% CI). Black represents an example of a correlation obtained with the data of a typical rat when the correlation between phase and synaptic slope of all the rats is significantly fitted by a sine function. The pseudocolor curve is shown when the correlation of the entire

long-term recordings of paired-pulse responses revealed an increase in PPR during REM compared with AW and QW (Friedman test $\chi^2_{(3)} = 13.1$, $p = 0.004$, effect size: 0.49; *post hoc* Dunn's test AW vs REM $p = 0.02$, QW vs REM $p = 0.04$, $n = 9$ rats). This result suggests that presynaptic mechanisms may contribute to the vigilance state-dependent modulation of PP-DG synaptic responses.

Vigilance state-dependent modulation of evoked responses at SC-CA1 synapse

The slope of SC-CA1 evoked synaptic responses was also deeply modulated during the sleep–wake cycle (Fig. 2*B*,*C*), with an increase during NREM and a decrease during AW and REM. The analysis from the entire group of 11 rats indicated a variation of fEPSP slopes at this synapse in the following direction: NREM > QW > [AW = REM] (Fig. 2*D*; Friedman test, $\chi^2_{(3)} = 27.1$, $p = 5.58e^{-06}$; *post hoc* Dunn's test: NREM vs REM $p < 0.001$, NREM vs AW $p < 0.001$, NREM vs QW $p < 0.001$, REM vs AW $p = 0.2$, REM vs QW $p = 0.01$, AW vs QW $p < 0.001$; effect size: $r = 0.88$ except for REM vs AW). Thus, in contrast with the PP-DG synapse, synaptic transmission at the SC-CA1 synapse was the highest during NREM.

We then determined the time course of synaptic changes at SC-CA1 synapse during the transitions between vigilance states (Fig. 2*F*). A rapid modulation of synaptic responses was found at several transitions between brain states. Fast synaptic changes were thus observed during transitions from NREM to REM (a 23% decrease in 1 min, Friedman test, $\chi^2_{(3)} = 29.72$, $p = 1.57e^{-06}$; *post hoc* Dunn's test $p < 0.0001$) and from REM to QW (Friedman test, $\chi^2_{(3)} = 29.5$, $p = 1{,}75e^{-06}$; *post hoc* Dunn's test $p = 0.003$). We also observed rapid synaptic changes for transitions between NREM and AW (Friedman test, $\chi^2_{(3)} = 22.74$, $p = 4{,}56e^{-05}$; *post hoc* Dunn's test $p < 0.009$). Thus, at the SC-CA1 synapse, rapid changes in fEPSP were observed during transitions between vigilance states, recalling those seen at the PP-DG synapse.

We next computed the evolution of the synaptic responses within each episode by dividing each episode by thirds (Fig. 2*G*). During REM episodes, the synaptic responses decreased rapidly between the first third and the second third ($p = 0.0006$), as at the PP-DG synapse. The analysis by thirds did not reveal any modulation during the other states.

To determine whether sleep induced gradual synaptic changes, we then quantified the effect of extended periods of sleep and wakefulness on synaptic responses. Figure 2*H* shows that an extended period of sleep did not modulate the slope of synaptic responses compared with an extended period of wakefulness (not significant, Wilcoxon Signed Rank test, $n = 11$ rats).

We then examined whether paired-pulse stimulation of evoked responses was modulated during the sleep–wake cycle (Fig. 2*I*). A PPF of synaptic response was observed at this synapse (in contrast with PP-DG synapse) that was increased during REM compared with QW and NREM (Friedman test $\chi^2_{(3)} = 17.55$, $p = 0.0005$, effect size: 0.71; *post hoc* Dunn's test: QW vs REM $p = 0.04$; NREM vs REM, $p = 0.04$, $n = 8$ rats). Moreover, an increase in PPF was also found during AW compared with QW (QW vs AW, $p = 0.04$). This result is consistent with a decrease in synaptic response during REM and AW because of a presynaptic mechanism.

Vigilance state-dependent modulation of evoked responses at hippocampal downstream synapses

The FX-mPFC synapse

The slope of evoked responses at the Fx-PFC synapse (P10 component, Fig. 3*B*,*C*) was also significantly modulated during the sleep–wake cycle in the following direction: [NREM = QW] > [REM = AW] (Fig. 3*E*; Friedman test, $\chi^2_{(3)} = 9.4$, $p = 0.04$; *post hoc* Dunn's test: NREM vs REM $p = 0.03$, NREM vs AW $p = 0.02$, NREM vs QW $p > 0.05$, REM vs AW $p > 0.05$, REM vs QW $p = 0.055$, AW vs QW $p = 0.008$; effect size: 0.36, n = 9 rats). Then, the modulation of synaptic slopes during vigilance state transitions was analyzed (Fig. 3*F*). We observed a rapid decrease in the synaptic response of NREM to REM (Friedman test, $\chi^2_{(3)} = 11.3$, $p = 0.009$; *post hoc* Dunn's test: $p = 0.006$) and an increase in response from REM to QW (Friedman test, $\chi^2_{(3)} = 10.73$, $p = 0.013$; *post hoc* Dunn's test: $p = 0.02$). The evolution of the evoked responses during each vigilance state episode was then computed by dividing each vigilance state episode by thirds (Fig. 3*G*). Evoked responses in the Fx-PFC pathway were not significantly modulated within a given vigilance state episode. To determine whether sleep induced gradual synaptic changes at this synapse, we then quantified the effect of extended periods of sleep on synaptic responses. Figure 3*H* shows that an extended period of sleep did not modulate the slope of synaptic responses compared with an extended period of wakefulness (not significant, Wilcoxon Signed Rank test, $n = 9$ rats). No modulation of PPF was also found during the sleep–wake cycle (Fig. 3*I*, $p > 0.05$, $n = 7$ rats).

The Fx-NAc synapse

The slope of evoked responses at the Fx-NAc synapse (P10 component, see Materials and Methods) was also modulated during the sleep–wake cycle as shown using estimation graphics from the full group of rats (Friedman test: $\chi^2_{(3)} = 16.6$, $p = 0.0008$; effect size: 0.50; $n = 11$ rats, Fig. 4*B*,*C*). In marked contrast with the PP-DG, SC-CA1, and Fx-PFC synapses, evoked responses at the Fx-NAc synapse increased during REM compared with NREM and wake (REM vs NREM: $p = 0.006$; REM vs AW: $p = 0.01$; REM vs QW: $p = 0.006$; AW vs QW: $p = 0.63$; AW vs NREM: $p = 0.21$; QW vs NREM: $p = 0.24$, Fig. 4*D*). Therefore, evoked responses at Fx-NAc synapse changed during vigilance states in the following direction: REM > [AW = NREM = QW].

We next computed the variation of synaptic responses during vigilance state transitions (Fig. 4*F*). We observed a fast modulation of evoked responses during transitions from NREM to REM (Friedman test, $\chi^2_{(3)} = 19.04$, $p = 0.0003$; *post hoc* Dunn's test: $p = 0.003$) and from REM to AW (Friedman test, $\chi^2_{(3)} = 17.95$, $p = 0.0005$; *post hoc* Dunn's test: $p = 0.0008$). The change in synaptic responses during vigilance state episodes was also assessed by dividing each episode by thirds (Fig. 4*G*). In marked contrast with the PP-DG and SC-CA1 synapses, evoked responses were not modulated during REM episodes ($p = 0.1933$ and $p = 0.0940$, respectively) at Fx-NAc

←

dataset is significantly fitted by a sine function (without *a priori* frequency band settings). The maximum synaptic slope is visualized by the color red while the minimum synaptic slope is visualized by blue. This curve illustrates the synaptic slope as a function of the phase of the oscillations. The statistics of the fitting curves (coefficient of determination and *p* value) are indicated in the graph. In AW, the maximum synaptic slope is found at the rising phase of theta oscillations, while the minimum is observed at its falling phase. Only the phase of theta oscillations is related to the synaptic slope, whatever the state of vigilance. Dark line indicates the randomized surrogate data generation of the entire dataset. Thickness of this line indicates the CI (500 randomizations). ***B***, Same as in ***A***, but for the SC-CA1 synapse. The maximum synaptic slope is located at the peak of the oscillation phase, except for AW where the maximum slope is observed at the falling phase of theta. Calibration: 250 ms, 0.1 mV.

synapse as at Fx-PFC synapse. To determine whether sleep induced gradual synaptic changes at the Fx-NAc synapse, the effect of extended periods of sleep on synaptic responses was assessed. Figure 4*H* shows that an extended period of sleep did not modulate the slope of synaptic responses compared with an extended period of wakefulness (not significant, Wilcoxon Signed Rank test, $n = 11$ rats). Finally, no modulation of PPF was found during the sleep–wake cycle (Fig. 4*I*, $p > 0.05$, $n = 7$ rats).

The Fx-Amy synapse

Responses to the Fx-Amy synapse were also modulated during the sleep–wake cycle (Friedman test, $\chi^2_{(3)} = 11.3$, $p = 0.009$, $n = 9$ rats, effect size: 0.42, Fig. 5*B–E*). Responses decreased during NREM compared with wakefulness (AW vs QW $p = 0.074$; AW vs NREM: $p = 0.012$; QW vs NREM: $p = 0.004$; NREM vs REM $p = 0.426$; REM vs AW: $p = 0.098$; REM vs QW: $p = 0.91$). We also observed a fast modulation of evoked responses during transitions from AW to QW (Friedman test, $\chi^2_{(3)} = 9.73$, $p = 0.02$, *post hoc* Dunn's test: $p = 0.03$) and from AW to NREM (Friedman test, $\chi^2_{(3)} = 14.1$, $p = 0.003$; *post hoc* Dunn's test: $p = 0.02$, Fig. 5*F*). The evolution of the evoked responses during each vigilance state episodes was then computed by dividing each vigilance state episode by thirds. As at Fx-NAc and Fx-PFC synapse (Fig. 5*G*), evoked responses in the Fx-Amy pathway were not significantly modulated during vigilance state episodes. Finally, to determine whether sleep induced gradual synaptic changes at the Fx-Amy synapse, we assessed the effect of extended periods of sleep (>30 min) on synaptic responses. Figure 5*H* shows that an extended period of sleep upregulated synaptic responses compared with an extended period of wakefulness ($p = 0.023$, Wilcoxon Signed Rank test).

Modulation of synaptic responses by the oscillation power

We next considered that synaptic changes we observed could be linked to local oscillations. Local brain states as characterized by spontaneous LFP oscillations are continuously changing on a short time scale (Kay and Frank, 2019). LFP oscillations recorded in the DG, CA1, PFC, NAc, and Amy (Fig. 6) showed prominent δ oscillations during NREM; although during REM, phasic theta waves were found in these structures that were associated with the prominent tonic theta oscillation (Meyer et al., 2018; Montgomery et al., 2008). It has been suggested that δ oscillations may modulate synaptic responses (Vyazovskiy et al., 2008; Chauvette et al., 2012). Moreover, the Communication Through Coherence hypothesis proposed that "postsynaptic rhythm modulates synaptic input gain" and that ongoing oscillations (e.g., γ waves) provide a flexible way to synchronize neuronal firing in distant areas during cognitive processes that involve them (Fries, 2005). Therefore, the link between prestimulus LFP oscillations and synaptic changes was assessed. We determined whether synaptic slopes could be influenced by the ongoing LFP oscillation immediately preceding the electrical stimulation triggering the evoked response. We then investigated the relationship between the magnitude of prestimulus oscillations and the slope of the synaptic responses (Fig. 6). Long-term recordings allow to compute correlations between synaptic slope and prestimulus LFP oscillation power for each vigilance state. The power of the prestimulus oscillations was quantified for slow oscillations (0.5-2 Hz), δ (2-4 Hz), theta (5-8 Hz), σ (9-14 Hz), low γ (38-45 Hz), and high γ (55-95 Hz); and then the *z*-scored power of these oscillations was correlated with the slope of each evoked response as shown in the Figure 6*A2* for theta waves. To perform multiple correlations, we used linear mixed-effect models (see Materials and Methods) (Bates et al., 2015), with the power of the frequency bands as fixed effects and animals as random effects. Thus, we determined whether the power of different frequency bands correlates with the modulation of the synaptic responses.

At the PP-DG synapse, during AW, synaptic responses were negatively correlated with the magnitude of the theta oscillations (R^2m = 0.042, $p = 1.231e^{-06}$, $n = 10$ rats; Fig. 6*A1*, *D*). We computed the marginal coefficient of determination (R^2m), which estimates the proportion of variance explained by the fixed-effects factors (i.e., oscillation power). During QW as well, synaptic slopes were negatively correlated with theta oscillations, but also with slow oscillations, δ, σ, and γ oscillations (R^2m = 0.093, $p = 6.166e^{-14}$) as for NREM (R^2m = 0.087, $p = 3.026e^{-12}$). In contrast, during REM, fEPSPs were positively correlated with the slow oscillations but negatively correlated with theta, σ, and γ oscillations (R^2m = 0.073, $p = 2.388e^{-14}$). To sum up, at this synapse, correlations between synaptic responses and oscillation power were found at all vigilance states and were predominantly negative.

At the SC-CA1 synapse, during AW, synaptic responses were positively correlated with the slow oscillations but negatively correlated with the low γ oscillations (R^2m = 0.031, $p = 0.0047$, $n = 10$ rats; Fig. 6*B*,*D*). In contrast, during REM, fEPSPs were positively correlated with the slow oscillations but negatively correlated with high γ oscillations (R^2m = 0.008, $p = 0.010$). Thus, at this synapse, correlations between synaptic responses and oscillation strength are only observed during AW and REM and the level of latter correlation was low.

At the Fx-PFC synapse, during AW, we found a positive correlation with σ (R^2m = 0.005 and $p = 0.0048$, $n = 9$ rats, Fig. 6*C*,*D*) and, during REM, a positive correlation with theta (R^2m = 0.019 and $p = 0.003$). At the Fx-NAc and Fx-Amy synapses, we found no significant correlation between the slope of the synaptic responses and the power of the oscillations, whatever the state of vigilance (Fig. 6*E*,*F*). Together, these results showed that the synaptic responses of the hippocampal pathways we studied were very weakly correlated with the magnitude of prestimulus oscillations, with the exception of the PP-DG synapse.

Correlation between the phase of LFP oscillations and synaptic changes

We next characterized synaptic changes related to the phase of the LFP oscillations at the time of stimulation (Figs. 7-9). We first correlated the synaptic slopes with the phase of the different oscillations using the 24 h database of each rat; then we averaged synaptic slopes (SEM) in each phase bin (bin size: 30°) for all rats. The graphs in Figure 7 show the correlation between the prestimulus oscillation phase and the synaptic slope at the PP-DG and SC-CA1 synapses for prominent wavebands (left to right: slow, δ, theta, σ, and γ oscillations). At each oscillation, the graphs are composed of superimposed curves of average data of the entire dataset (2 cycles from −180 to 510°), the sinusoidal fitting curve of the average (thick red line, the 95% CI is represented by the curve thickness), the surrogates of the dataset (thick black curve; 95% CI is represented by the curve thickness), and the representation of synaptic slopes related to the phase (pseudo-color curve). The data from 1 animal (thin black line) are shown superimposed on the other curves, which show a similar phase relationship to the whole population. At the PP-DG synapse (Fig. 7*A*), synaptic slopes were significantly linked to

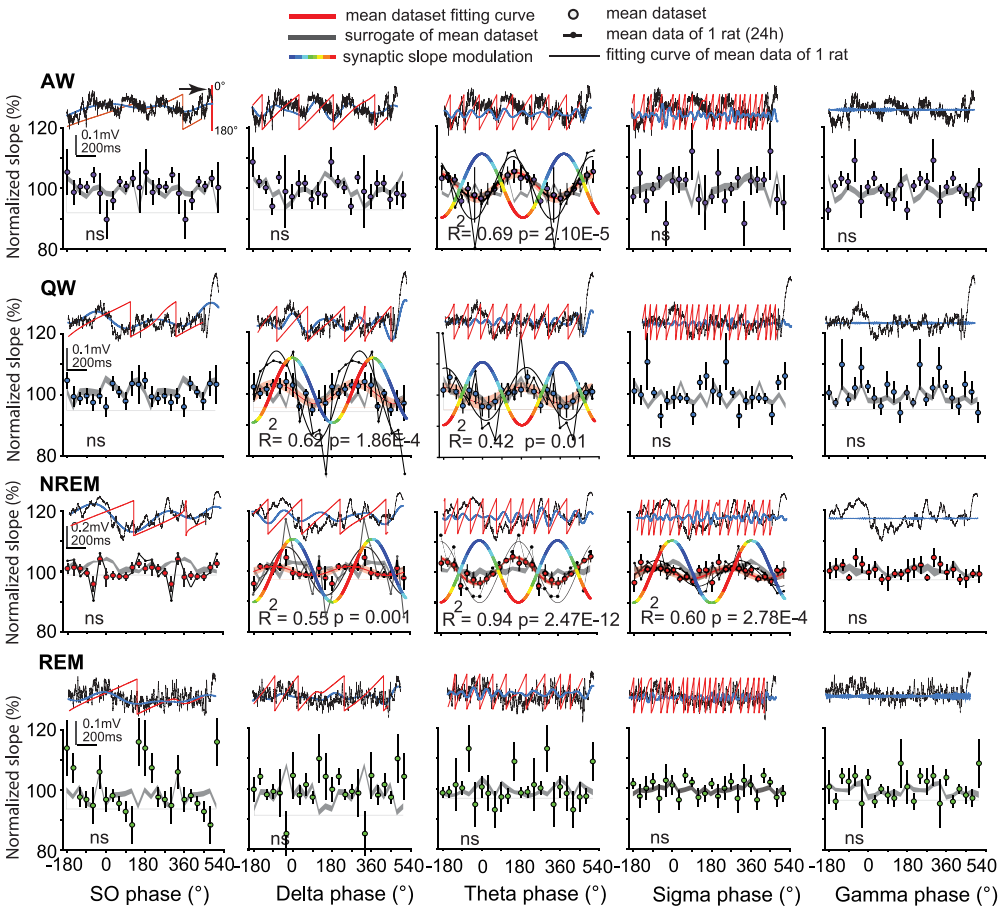

Figure 8. Correlation between the phase of LFP oscillations and the synaptic changes at the Fx-PFC synapse. At the Fx-PFC synapse, correlation between the synaptic slope by the phase of LFP oscillations during QW (blue). Top, Superimposed single traces representing the raw data (black), the filtered data in the waveband (blue), and the phase (red). Black arrows indicate the time of the electrical stimulation and synaptic response. Bottom, Superimposed correlations (gray dots) between the phase (from −180° to 540°) and the synaptic slopes of the database over 24 h ($n = 10$ rats). On the same graphs, average correlation of the entire dataset (purple dots for AW, blue dots for QW, red dots for NREM, and green dots for REM) and the superimposed fitting curve (red with 95% CI). The randomized surrogate data generation of the entire dataset is represented by a dark line and the CI by the thickness of this line (500 randomizations). Calibration: 250 ms, 0.1 mV.

phase for theta oscillations. The value of the coefficient of determination was moderate ($R^2 \sim 0.5$), and the phase dependent modulation of the synaptic slope were low and close to the surrogate. During wakefulness and sleep, the maximum of synaptic slope was located at the ascending phase of theta (red in the pseudo-color curve). At the SC-CA1 synapse (Fig. 7*B*), synaptic slopes were also linked to theta phase during all states. Although the value of the coefficient of determination was high ($R^2 > 0.6$) indicating a good fit between the model and the averaged data, the modulation of the synaptic slope is low and close to the surrogate, except for the σ oscillations during NREM and QW. The maximum of the synaptic slopes was located at the peak of theta (for QW and sleep) or at the theta descending phase (for AW). In addition, at this synapse, correlations were observed between synaptic slopes and σ (during QW and NREM) and γ oscillation (during REM). At the Fx-PFC synapse, correlations with δ, theta, and σ oscillations were found during NREM and QW (Fig. 8). However, these synaptic phase-dependent changes in oscillations were small, except for theta oscillations during NREM. The maximum of the synaptic slopes was located at the trough of theta and at the δ and σ ascending phase (for AW). At the Fx-Nac synapse, several correlations were found, in particular for theta and γ oscillations (Fig. 9*A*). These correlations were weak, except for theta and γ during QW. Finally, at the synapse Fx-Amy, we also found synaptic slope and phase relationship, especially for theta and γ (Fig. 9*B*). Together, these results thus suggested the existence of links between synaptic changes and phase in particular during sleep. During NREM, synaptic slopes were frequently correlated with the phase of slow, δ, and σ oscillations but also with theta wave. During REM, synaptic slopes were more correlated with the phase of theta and γ oscillations. Moreover, for a given synapse, similar synaptic slope–phase relationship was frequently observed for theta, σ, and γ at all states, except for AW (i.e., the maximum of the synaptic slope was at the peak of theta at the SC-CA1 synapse for wakefulness and sleep and at the trough of theta at the Fx-PFC synapse for all states, see Fig. 12*B*). These phase-dependent modulations of synaptic strength were, however, small compared with that of vigilance states.

Correlation between theta frequency and synaptic responses

We then examined whether synaptic responses were linked to the variation in theta frequency. The correlation between theta frequency and synaptic responses was computed at each synapse (Fig. 10). At the PP-DG synapse, a negative correlation was found between theta frequency and synaptic slope, mainly during AW and REM (Fig. 10*A*, left and middle). The correlation was weaker in QW than in AW and REM (Fig. 10*A*, right). At the SC-CA1 synapse, a negative correlation between theta frequency and synaptic slope was also found in AW and sleep but not in QW (Fig. 10*B*). At the Fx-PFC synapse, synaptic slopes were negatively correlated with theta frequency selectively during

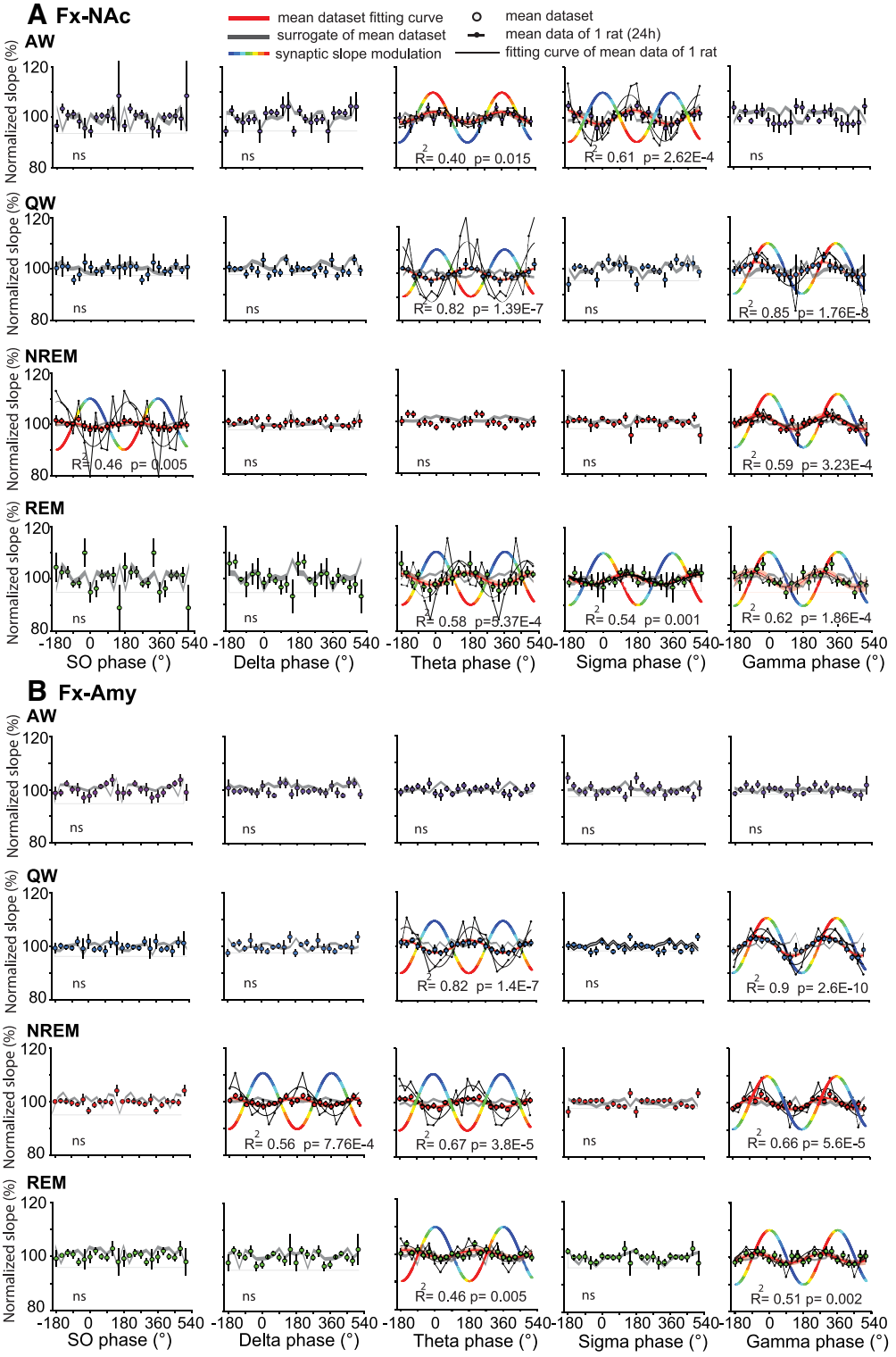

Figure 9. Correation between the phase of LFP oscillations and the synaptic changes at the Fx-NAc and Fx-Amy synapses. ***A***, At the Fx-NAc synapse, correlation between the synaptic slope by the phase of LFP oscillations during AW (purple), QW (blue), NREM sleep (red), and REM sleep (green). Top, Superimposed single traces representing the raw data (black), the filtered data in the waveband (blue), and the phase (red). Black arrows indicate the time of the electrical stimulation and synaptic response. Bottom, Superimposed correlations (gray dots) between the phase (from −180° to 540°) and the synaptic slopes of the database over 24 h ($n = 10$ rats). On the same graphs, average correlation of the entire dataset (purple dots for AW, blue dots for QW, red dots for NREM, and green dots for REM) and the superimposed fitting curve (red with 95% CI). The randomized surrogate data generation of the entire dataset is represented by a dark line and the CI by the thickness of this line (500 randomizations). ***B***, Same as in ***A***, but for the Fx-Amy synapse.

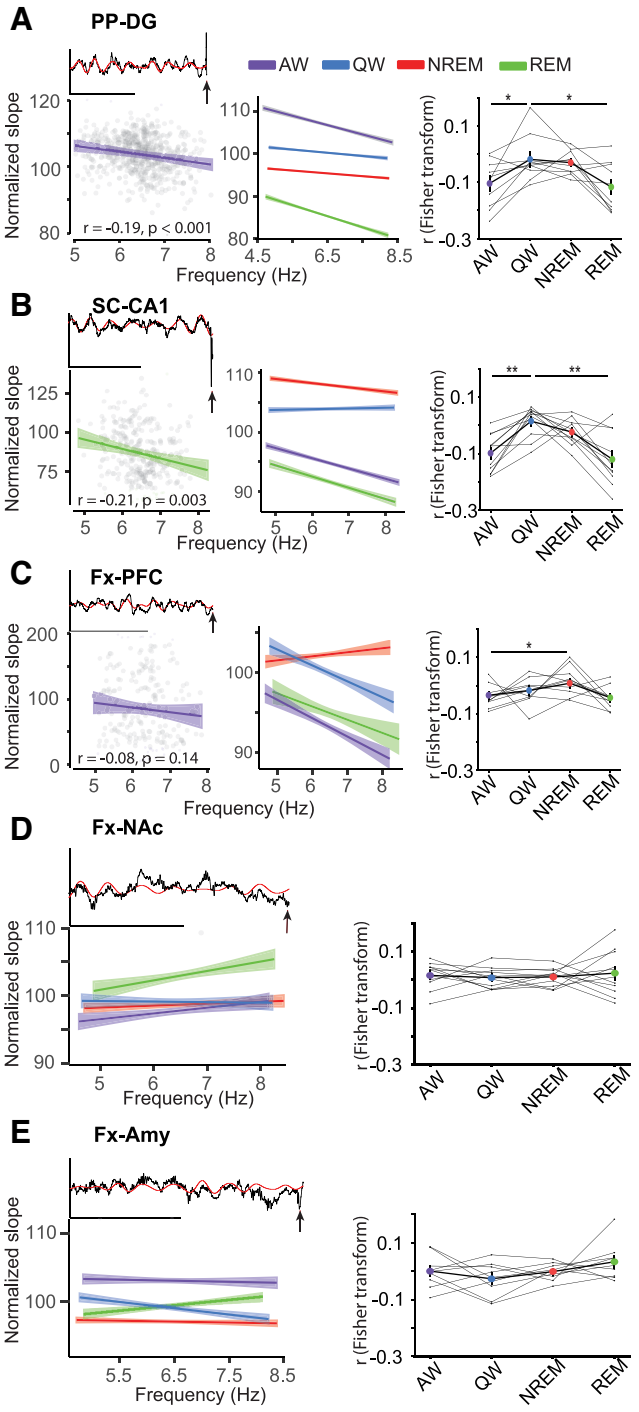

Figure 10. Correlation between the theta frequency and the synaptic responses. ***A***, At the PP-DG synapse, theta frequency and synaptic slope were negatively correlated. Top left, Sample data with the raw trace (black) and the filtered theta band (red). Bottom left, Correlation between theta frequency and synaptic slope during AW for 1 rat. Arrow indicates the synaptic response. Middle, The correlations were calculated with the entire dataset (AW: $r = -0.10$, $p = 4.6e^{-15}$; QW: $r = -0.03$, $p = 0.02$; NREM: $r = -0.03$, $p = 0.003$; REM: $r = -0.11$, $p = 8.0e^{-09}$; $n = 10$ rats). Only the linear fitting curves (and their CI) are shown for the different vigilance states. Right, The correlation coefficient (corrected with Fisher *z* transformation) of all rats was weaker in QW than in AW and REM (Friedman test, $\chi^2_{(3)} = 10.92$, $p = 0.0018$, followed by *post hoc* Dunn's test, AW vs QW $p = 0.03$; REM vs QW $p = 0.04$). ***B***, At the SC-CA1 synapse, a negative correlation between theta frequency and synaptic slope was found in AW and sleep but not in QW. Left, Correlation between theta frequency and synaptic slope during REM for 1 rat. Middle, Correlations during AW: $r = -0.08$, $p < 2.2e^{-16}$; QW: $r = -0.006$, $p = 0.2$; NREM: $r = -0,04$, $p < 2.2e^{-16}$; REM: $r = -0.09$, $p < 2.2e^{-16}$, $n = 11$ rats. Right, The correlation coefficient (corrected with Fisher *z* transformation) of all rats was weaker in QW than in AW and REM (Friedman test, $\chi^2_{(3)} = 21.44$, $p = 8.54e^{-5}$, *post hoc* Dunn's test, AW vs QW $p = 7.27e^{-4}$; REM vs QW $p = 8.74e^{-4}$). ***C***, At the Fx-PFC synapse, responses were negatively correlated with theta frequency in wakefulness but not in sleep. Left, Correlation between theta frequency and synaptic slope during AW for 1 rat. Middle, Correlations during AW: $r = -0.04$, $p < 0.006$; QW: $r = -0.03$, $p = 0.01$; NREM: $r = -0.009$, $p = 0.4$; REM: $r = -0.03$, $p = 0.15$, $n = 9$ rats. Right, A difference in correlation coefficients was observed between AW and NREM (Friedman test, $\chi^2_{(3)} = 10.73$, $p = 0.013$, *post hoc* Dunn's test $p = 0.02$). ***D***, No correlation was found between the theta frequency and the synaptic slope at the Fx-NAc synapse (AW: $r = 0.015$, $p = 0.24$; QW: $r = -0.002$, $p = 0.9$; NREM: $r = 0.006$, $p = 0.5$; REM: $r = 0.02$, $p = 0.14$; $n = 11$ rats). No significant correlation was observed at this synapse between vigilance states (Friedman test, $\chi^2_{(3)} = 0.71$, $p = 0.87$). ***E***, No correlation was found between the theta frequency and the synaptic slope at the Fx-Amy synapse (AW: $r = -0.003$, $p = 0.74$; QW: $r = -0.03$, $p = 0.06$; NREM: $r = -0.005$, $p = 0.6$; REM: $r = 0.03$, $p = 0.09$; $n = 9$ rats). No significant correlation was observed at this synapse between vigilance states (Friedman test, $\chi^2_{(3)} = 4.06$, $p = 0.25$). Calibration: 0.5 mV, 500 ms. $^*p < 0.05$.

AW (Fig. 10*C*). In contrast, at the Fx-NAc and Fx-Amy synapses, synaptic slopes did not appear to be linked to theta frequency, whatever the state of vigilance (Fig. 10*D*,*E*). Thus, these results showed the existence of a low-level negative correlation between prestimulus theta frequency and synaptic slopes at the PP-DG, SC-CA1, and Fx-PFC synapses that contributes only weakly to explain the variance in the responses at these synapses.

Covariation of the synaptic responses at the three hippocampal efferent synapses

We next examined whether there was some degree of covariation of the responses at these synapses. We took advantage of the experimental design that evoked simultaneous responses at the three hippocampal efferent pathways to determine whether the synaptic responses at these synapses covaried together at each stimulation of the Fx (i.e., Fx-PFC, Fx-NAc, Fx-Amy; Fig. 11*A*, inset). Figure 11*A* shows the superimposed time course of the responses at the Fx-PFC, Fx-NAc, and Fx-Amy synapses for a rat. The 2 × 2 correlation between these synapses revealed a high degree of correlation between the responses of the Fx-PFC and Fx-NAc synapses, in contrast to the correlations between the responses of the Fx-PFC and Fx-Amy synapses and between the responses of the Fx-NAc and Fx-Amy synapses (Fig. 11*A*, left). We next computed the correlation coefficient of the correlations of the synaptic slopes for two-by-two synapses for each vigilance state (Fig. 11*B*). We did not observe a modulation of the covariation of synaptic responses during the sleep–wake cycle (Fig. 11*C*). When the correlation was calculated for each animal on all synaptic responses, whatever the state of vigilance, it appeared that the correlation between the synaptic slopes of the Fx-PFC and Fx-NAc synapses was much higher than the correlation between the Fx-PFC and Fx-Amy synapses and the correlation between the Fx-NAc and Fx-Amy synapses (Fig. 11*D*, correlation between Fx-PFC and Fx-NAc: $r = 0.88 \pm 0.15$; correlation between Fx-PFC and Fx-Amy: $r = 0.06 \pm 0.03$; and correlation between Fx-NAc and Fx-Amy: $r = 0.07 \pm 0.02$; $n = 8$ rats). We then asked what contribution a common covariation between the responses of these three synapses could make to these correlations. To test this, we computed the partial correlation between the responses of these three synapses and observed that the correlation coefficients between the Fx-PFC and Fx-NAc synapses was almost identical as that was obtained previously for the 2 × 2 correlations (correlation between Fx-PFC and Fx-NAc: $r = 0.88 \pm 0.15$; correlation between Fx-PFC and Fx-Amy: $r = 0.03 \pm 0.03$; correlation between Fx-NAc and

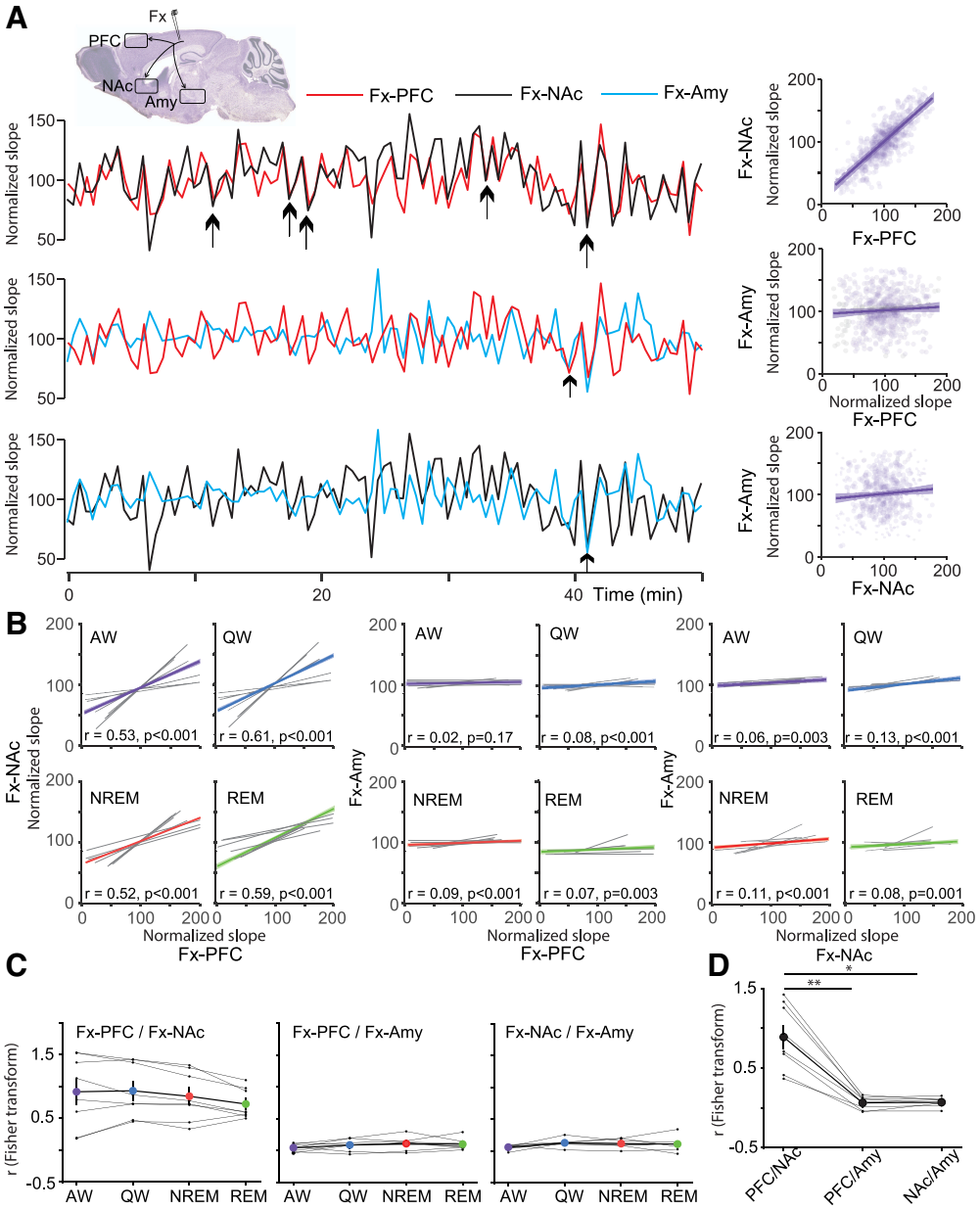

Figure 11. Covariation of the synaptic responses between the three hippocampal efferent pathways. ***A***, Correlation of the synaptic slopes between pairs of synapses during the sleep–wake cycle. The rationale for the experiment is presented in the inset (top) on a sagittal section of the rat brain that illustrates the site of electrical stimulation in the Fx corresponding to the hippocampal axons that connect neurons in the PFC, the NAc, and the Amy. Left, Top to bottom, Time course of synaptic slopes (normalized) for the three efferent pathways of a rat for 50 min. The evolution of the synaptic slopes is superimposed to illustrate the covariation of the responses. Arrows indicate covariations. Right, Top to bottom, Graphs represent the correlations between the slope of Fx-PFC and Fx-NAc synapses (top), between the slope of Fx-NAc and Fx-Amy synapses (middle), and between the slope of Fx-PFC and Fx-Amy synapses (bottom) and the linear fitting curve with the CI (same data as in left). ***B***, Dark gray linear fitting curves indicate 2 × 2 correlations of the slopes of the three synapses from 1 rat during the vigilance states (AW, QW, NREM, and REM). Colored curves represent the linear fitting curve (with the CI, the Pearson correlation coefficient [*r*], and the *p* value) of the data correlations obtained from 8 rats. ***C***, The correlation coefficients (*r* coefficient corrected with Fisher *z* transformation; Fisher transformation explains why values are >1) were not modulated by the sleep–wake cycle ($p > 0.05$, Friedman test, $n = 8$ rats). Left to right, For each vigilance state, the slope of the linear fitting curves of the correlations between the responses of Fx-NAc and Fx-PFC synapses, between Fx-Amy and Fx-PFC synapses, and between Fx-NAc and Fx-Amy synapses. ***D***, Comparison of the correlations of the synaptic slopes between the three pairs of synapses regardless of the vigilance states (correlation between Fx-PFC and Fx-NAc synapses [$r = 0.88 \pm 0.15$]; correlation between Fx-PFC and Fx-Amy synapses [$r = 0.06 \pm 0.03$]; correlation between Fx-NAc and Fx-Amy synapses [$r = 0.07 \pm 0.02$], $n = 8$ rats, 14,016 responses for the three synapses). The level of correlation was much higher for the Fx-NAc/Fx-PFC pair than for the Fx-Amy/Fx-PFC and Fx-NAc/Fx-Amy pairs (Friedman test, $\chi^2_{(2)} = 12.56$, $p = 0.0018$, followed by *post hoc* Dunn's test, $p = 0.002$ between the correlation Fx-PFC and Fx-NAc synapses and the correlation Fx-PFC and Fx-Amy synapses; $p = 0.016$ between the correlation Fx-PFC and Fx-NAc synapses and the correlation Fx-NAc and Fx-Amy synapses). $^{**}p < 0.01$. $^{*}p < 0.05$.

Fx-Amy: $r = 0.01 \pm 0.03$). To summarize, these results revealed a covariation of synaptic responses between the Fx-PFC and the Fx-NAc synapses which did not covariate with the Fx-Amy synaptic responses and that was not modulated during the sleep–wake cycle.

Discussion

This work shows that brain states differentially modulate synaptic transmission of pathways projecting to, within, and from the Hpc. We discovered that the sleep–wake cycle induces two types of synaptic changes: a rapid modulation mainly at transitions

between vigilance states in five hippocampal connections and a change after extended periods of sleep for PP-DG and Fx-Amy synapses. A feature of the synaptic changes we observed is their large variability. This variability was not because of electrode movements since we control the fEPSPs during several days. Brain temperature changes cause synaptic variability (Moser et al., 1994). However, temperature is unlikely to explain the synapse-specific modulations since in the same structure, the PP-DG and SC-CA1 synapses behave very differently.

We found that, during wakefulness, responses at the PP-DG synapse were increased compared with sleep. This result expands Winson and Abzug (1977) that did not show the changes in response between AW and QW and between REM and NREM. Synaptic changes could be caused by state-dependent neuromodulation (Lee and Dan, 2012). Indeed, noradrenaline depletion was found to abolish the wake-NREM-dependent modulation of responses at the PP-DG synapse (Dahl et al., 1983). Given the low level of noradrenaline release during NREM compared with AW and the lack of noradrenaline during REM, our result could thus involve a β receptor-dependent facilitation of synaptic transmission during wakefulness (Haas and Rose, 1987). The synaptic changes during transitions between vigilance states could be linked to fast modulation of noradrenergic signaling as in the thalamus (Osorio-Forero et al., 2021).

In contrast, at the SC-CA1 synapse, we found an enhancement of responses during NREM. Leung (1980) showed that SC-CA1 synaptic responses are higher during NREM than during AW, but not between NREM and QW. This author found a decrease of SC-CA1 fEPSPs during REM compared with NREM and QW, but not compared with AW. Here, with many more rats, we found that responses were the lowest during REM. We reveal an increase in PPF in REM, suggesting a presynaptic mechanism for the decrease in synaptic slope, although a differential recruitment of inhibition during vigilance states could modulate PPF. This reduction in glutamate release could be because of the cholinergic activity during REM and AW (Marrosu et al., 1995; Howe et al., 2017). This cholinergic signaling during REM and AW would thus inhibit the hippocampal network by activating presynaptic muscarinic receptors at the SCs (Hasselmo and Schnell, 1994).

Surprisingly, an increase in Fx-NAc transmission was observed during REM compared with the other vigilance states. This increase could be linked to postsynaptic factors since PPF is not modulated during REM. The increased burstiness of VTA neurons observed during REM (Dahan et al., 2007) could increase dopaminergic signaling in the NAc during this state. Thus, during REM, dopamine release may activate receptors located on spiny neurons, thereby enhancing AMPA-mediated synaptic responses (Goto and Grace, 2008). Thus, our result suggests an involvement of REM in reward systems, including the NAc to enhance memory consolidation (Perogamvros and Schwartz, 2012).

Our results also show that extended periods of sleep lead to different synaptic changes at different synapses. In the majority of synapses, extended periods of sleep have no effect on synaptic responses in the visual and prefrontal cortices (Cary and Turrigiano, 2021). At the PP-DG synapse, however, we observe a downregulation, as predicted by the Synaptic Homeostasis Hypothesis. This synaptic change is weak (<10%) compared with those found at transitions between vigilance states (which are often higher than 10%) and to callosal connections (Vyazovskiy et al., 2008). On the opposite, we observe a sleep-dependent upregulation of the Fx-Amy responses, as shown for thalamo-cortical connections (Chauvette et al., 2012). Thus, these last two synapses (PP-DG and Fx-Amy), which are the only ones to show an increase in synaptic responses during AW compared with other vigilance states, have opposite regulations after prolonged sleep periods.

What could be the consequence of these sleep-dependent synaptic changes? These changes may be ideally optimized for memory consolidation processes during the sleep–wake cycle. Upon wakefulness, at the beginning of the cycle, synaptic strength increases at the PP-DG synapse to consolidate newly acquired information. Then, during subsequent NREM, responses would be increased at the intrahippocampal synapse to allow this information to be transferred to the cortex to be consolidated. Such consolidation could be further reinforced during NREM and QW at the Fx-PFC synapse. In addition, consolidation would be facilitated in the NAc during REM and in the Amy during AW for storage of reward based and/or emotional events.

Our results also reveal that changes in oscillation power modulate synaptic responses (Fig. 12). PP-DG responses seem to be more modulated by oscillation power than other synapses. At this synapse, several types of waves, except slow oscillations, were negatively correlated with synaptic slopes. Correlations were found for theta during all vigilance states. Granular cell recordings show that spontaneous EPSPs, which are mainly generated at the PP-DG synapse, are coherent with theta (Pernia-Andrade and Jonas, 2014). Since the PP-DG responses are characterized by a PPD, it is likely that the increase in theta power, corresponding to higher excitatory drive, leads to a depression of the subsequent synaptic responses. Theta-dependent modulation may contribute to the integration of different information conveyed by theta in granular cells. In contrast, slow oscillations are positively correlated with responses during REM at the PP-DG synapse but also at the SC-CA1 synapse. This effect may seem surprising given that slow waves are not predominant during this state. However, at the beginning of REM episodes, DG and CA1 slow waves show a higher power than later. This transient substate at the beginning of REM episodes corresponds to the period when fEPSPs are greater (Figs. 1*H*, 2*G*). This result suggests that the last two-thirds of a REM episode may exert a role, perhaps of reorganizing excitability, that could be related to the redistribution of interneuron activity (Grosmark et al., 2012).

The phase of oscillations also modulates synaptic responses. Phase-dependent changes are small in amplitude and are only separated from the surrogates to some synapses and for some oscillations. The main explanation is that some rats out of the dataset show a significant correlation between synaptic changes and phase of the oscillations or that there is an important "jitter" in the phase relationship between rats. Thus, given that the surrogates and the fitting curve are calculated on the dataset, only a few significant results emerge from the average. At the SC-CA1 synapse, slope modulation at theta peak during sleep and QW coincides with the minimum discharge for pyramidal cells and the maximum discharge for several types of interneurons (Klausberger and Somogyi, 2008). Thus, the modulation of excitatory and inhibitory neuron activity in CA1 could contribute to enhance the driving force for SC-CA1 fEPSPs evoked at peak theta compared with those evoked at trough. In anesthetized rats, responses at this synapse are maximal during the

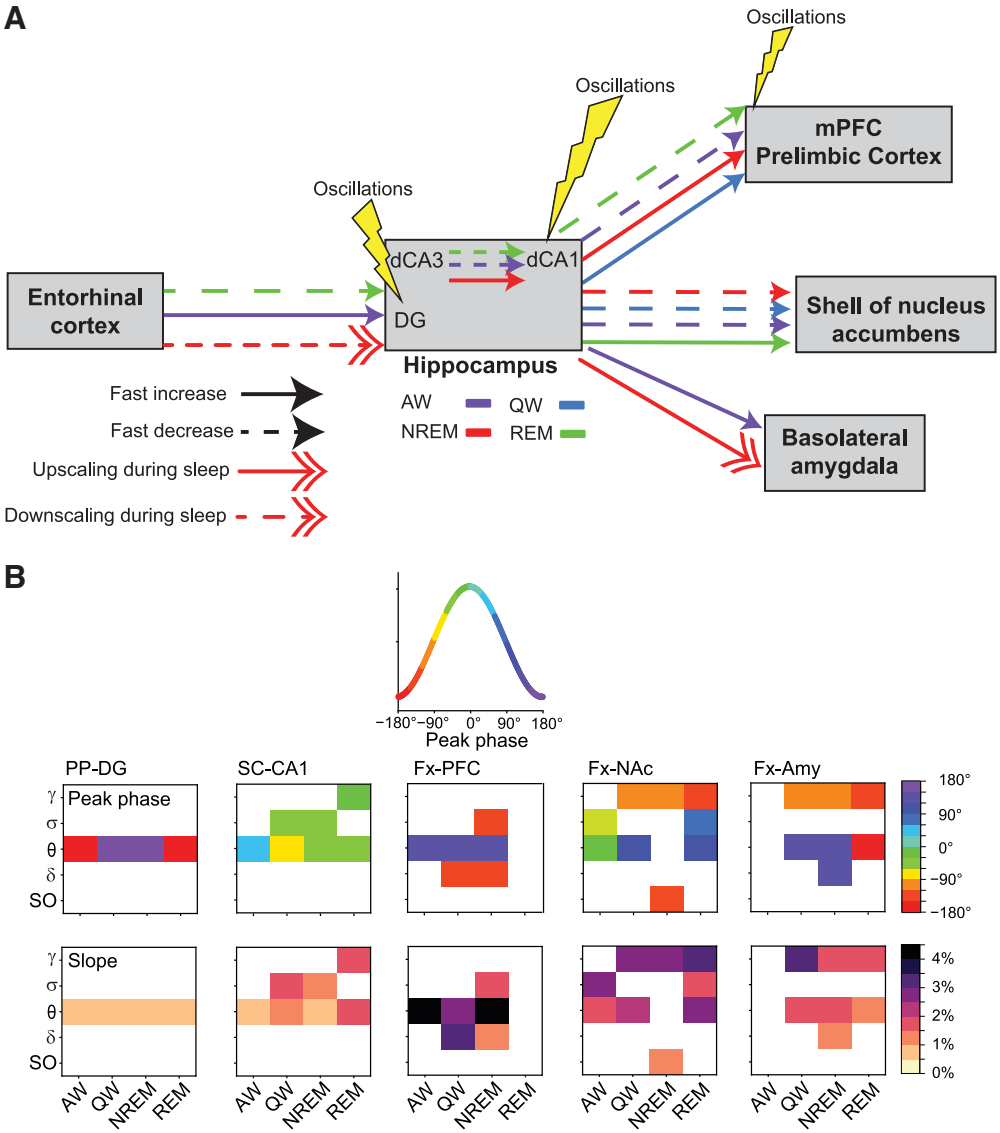

Figure 12. ***A***, Schematic representation of the main results. This diagram represents that the two states of wakefulness and sleep exert very different roles on synaptic responses at different timescales. REM rapidly decreases synaptic responses at all synapses, except the one between the Hpc and the NAc (Fx-NAc synapse) where it is increased. NREM increases synaptic responses at the SC-CA1 synapse and the synapse between the Hpc and the mPFC. This suggests a facilitation of information transfer to these two synapses during this sleep state according to the Active System Consolidation hypothesis (Rasch and Born, 2013). At a different timescale, extended periods of sleep induced a downregulation or an upregulation of synaptic responses at only two synapses, PP-DG and Fx-Amy, respectively. Finally, the responses of the three cortical synapses (PP-DG, SC-CA1, and Fx-PFC) were more modulated by the power and the phase of LFP oscillations than those of the two subcortical synapses (Fx-NAc and Fx-Amy). ***B***, Schema representing the main correlation results between the phase of prestimulus LFP oscillations and the slope of synaptic responses. This correlation is significantly fitted by a sinusoidal function for several synapses and for several frequency bands, including theta, σ, and γ bands (average of 24 h recordings of all rats). Inset, Color code of the phase of the oscillations (i.e., red and purple represents the phase trough). Top, The matrix row represents the phase of the oscillation for the synaptic slope maximum. For the PP-DG synapse, the maximum tends to be located at the trough of the theta oscillation; while for the SC-CA1 synapse, the maximum is at the peak of most theta, σ, and γ oscillations. Bottom, The matrix row represents the synaptic slope maximum modulated by the phase of the oscillations. At the Fx-PFC synapse, δ and theta oscillations modulate the synaptic slope to a greater extent than at other synapses, such as the PP-DG synapse.

descending phase of theta as we find for AW (Schall et al., 2008). Interestingly, at the SC-CA1 and Fx-PFC synapses, phase-synaptic response relationships are found for δ, σ, and theta during NREM. This phase-dependent regulation of synaptic changes may contribute to sleep-dependent consolidation by reinforcing phase coherence between the Hpc and the PFC. At the Fx-PFC synapse, during NREM, the maximum synaptic response is located at the ascending phase of δ and σ. This phase relationship could regulate synaptic changes during upstates and downstates. It would be important to determine the relationship between ripples, which are linked to upstates, and fEPSPs. Surprisingly, at the Fx-NAc synapse, responses are correlated with theta and γ phase during REM. These phase-dependent changes emphasize the role of the Fx-NAc synapse during REM-dependent memory processing. Finally, we reveal the specific phase-synaptic change relationship for theta or γ at a synapse, whatever the vigilance state as shown at the Fx-NAc and Fx-Amy synapses (Figs. 9, 12*B*). It is possible that these synapses present a selective phase preference because of intrinsic ionic mechanisms (Izhikevich et al., 2003) activated by oscillations through ephaptic coupling (Anastassiou et al., 2011).

Our results also reveal a covariation of synaptic responses at the Fx-PFC and Fx-NAc pathways. In contrast, we did not observe any covariation between the Fx-Amy synapse and the

Fx-PFC and Fx-NAc synapses, whatever the state. Interestingly, pyramidal cells in the Hpc send axons that bifurcate into branches that contact neurons of the PFC, the NAc, and the Amy (Ciocchi et al., 2015). Therefore, a variation in excitability at one of these multibranch axons could explain the covariation of synaptic responses. The covariation of responses between Fx-PFC and Fx-NAc pathways may underlie a synchronization of neuronal activity in the PFC and the NAc, a factor that may help the information transfer from the Hpc to these structures.

In conclusion, our findings reveal that five hippocampal synapses behave differently during vigilance states. Oscillations also contribute to this differential modulation, albeit at a weaker level. These synaptic changes, associated with state-dependent forms of synaptic plasticity (Seibt and Frank, 2019), may allow a sequential integration of information during wakefulness and offline memory processing during sleep.

References

Anastassiou CA, Perin R, Markram H, Koch C (2011) Ephaptic coupling of cortical neurons. Nat Neurosci 14:217–223.

Andersen P, Silfvenius H, Sundberg SH, Sveen O (1980) A comparison of distal and proximal dendritic synapses on CA1 pyramids in guinea-pig hippocampal slices in vitro. J Physiol 307:273–299.

Bates D, Mächler M, Bolker B, Walker S (2015) Fitting linear mixed-effects models using lme4. J Stat Soft 67:1–48.

Boeijinga PH, Mulder AB, Pennartz CM, Manshanden I, Lopes da Silva FH (1993) Responses of the nucleus accumbens following fornix/fimbria stimulation in the rat: identification and long-term potentiation of mono- and polysynaptic pathways. Neuroscience 53:1049–1058.

Cary BA, Turrigiano GG (2021) Stability of neocortical synapses across sleep and wake states during the critical period in rats. Elife 10:e66304.

Chauvette S, Seigneur J, Timofeev I (2012) Sleep oscillations in the thalamocortical system induce long-term neuronal plasticity. Neuron 75:1105–1113.

Ciocchi S, Passecker J, Malagon-Vina H, Mikus N, Klausberger T (2015) Selective information routing by ventral hippocampal CA1 projection neurons. Science 348:560–563.

Colino A, Malenka R (1993) Mechanisms underlying induction of long-term potentiation in rat medial and lateral perforant paths in vitro. J Neurophysiol 69:1150–1159.

Dahan L, Astier B, Vautrelle N, Urbain N, Kocsis B, Chouvet G (2007) Prominent burst firing of dopaminergic neurons in the ventral tegmental area during paradoxical sleep. Neuropsychopharmacology 32:1232–1241.

Dahl D, Bailey WH, Winson J (1983) Effect of norepinephrine depletion of hippocampus on neuronal transmission from perforant pathway through dentate gyrus. J Neurophysiol 49:123–133.

Frank MG (2015) Sleep and synaptic plasticity in the developing and adult brain. Curr Top Behav Neurosci 25:123–149.

Fries P (2005) A mechanism for cognitive dynamics: neuronal communication through neuronal coherence. Trends Cogn Sci 9:474–480.

Gervasoni D, Lin SC, Ribeiro S, Soares ES, Pantoja J, Nicolelis MA (2004) Global forebrain dynamics predict rat behavioral states and their transitions. J Neurosci 24:11137–11147.

Goto Y, Grace AA (2008) Limbic and cortical information processing in the nucleus accumbens. Trends Neurosci 31:552–558.

Grosmark AD, Mizuseki K, Pastalkova E, Diba K, Buzsáki G (2012) REM sleep reorganizes hippocampal excitability. Neuron 75:1001–1007.

Haas HL, Rose GM (1987) Noradrenaline blocks potassium conductance in rat dentate granule cells in vitro. Neurosci Lett 78:171–174.

Hasselmo M, Schnell E (1994) Laminar selectivity of the cholinergic suppression of synaptic transmission in rat hippocampal region CA1: computational modeling and brain slice physiology. J Neurosci 14:3898–3914.

Howe WM, Gritton HJ, Lusk NA, Roberts EA, Hetrick VL, Berke JD, Sarter M (2017) Acetylcholine release in prefrontal cortex promotes gamma oscillations and theta-gamma coupling during cue detection. J Neurosci 37:3215–3230.

Izhikevich EM, Desai NS, Walcott EC, Hoppensteadt FC (2003) Bursts as a unit of neural information: selective communication via resonance. Trends Neurosci 26:161–167.

Kay K, Frank LM (2019) Three brain states in the hippocampus and cortex. Hippocampus 29:184–238.

Klausberger T, Somogyi P (2008) Neuronal diversity and temporal dynamics: the unity of hippocampal circuit operations. Science 321:53–57.

Lee SH, Dan Y (2012) Neuromodulation of brain states. Neuron 76:209–222.

LeGates TA, Kvarta MD, Tooley JR, Francis TC, Lobo MK, Creed MC, Thompson SM (2018) Reward behaviour is regulated by the strength of hippocampus-nucleus accumbens synapses. Nature 564:258–262.

Leung LS (1980) Behavior-dependent evoked potentials in the hippocampal CA1 region of the rat: I. Correlation with behavior and EEG. Brain Res 198:95–117.

Levita L, Dalley JW, Robbins TW (2002) Disruption of Pavlovian contextual conditioning by excitotoxic lesions of the nucleus accumbens core. Behav Neurosci 116:539–552.

Maingret N, Girardeau G, Todorova R, Goutierre M, Zugaro M (2016) Hippocampo-cortical coupling mediates memory consolidation during sleep. Nat Neurosci 19:959–964.

Manabe T, Wyllie DJ, Perkel DJ, Nicoll RA (1993) Modulation of synaptic transmission and long-term potentiation: effects on paired pulse facilitation and EPSC variance in the CA1 region of the hippocampus. J Neurophysiol 70:1451–1459.

Marrosu F, Portas C, Mascia M, Casu M, Fa M, Giagheddu M, Imperato A, Gessa G (1995) Microdialysis measurement of cortical and hippocampal acetylcholine-release during sleep–wake cycle in freely moving cats. Brain Res 671:329–332.

Meyer G, Carponcy J, Salin PA, Comte JC (2018) Differential recordings of local field potential: a genuine tool to quantify functional connectivity. PLoS One 13:e0209001.

Missaire M, Fraize N, Comte JC, Truchet B, Parmentier R, Salin PA, Malleret G (2021) Working and reference memory tasks trigger opposed long-term synaptic changes in the rat dentate gyrus. Cereb Cortex 31:2980–2992.

Montgomery SM, Sirota A, Buzsáki G (2008) Theta and gamma coordination of hippocampal networks during waking and rapid eye movement sleep. J Neurosci 28:6731–6741.

Moser EI, Moser MB, Andersen P (1994) Potentiation of dentate synapses initiated by exploratory learning in rats: dissociation from brain temperature, motor activity, and arousal. Learn Mem 1:55–73.

Mulder AB, Arts MP, Lopes da Silva FH (1997) Short- and long-term plasticity of the hippocampus to nucleus accumbens and prefrontal cortex pathways in the rat, in vivo. Eur J Neurosci 9:1603–1611.

Mulder AB, Hodenpijl MG, Lopes da Silva FH (1998) Electrophysiology of the hippocampal and amygdaloid projections to the nucleus accumbens of the rat: convergence, segregation, and interaction of inputs. J Neurosci 18:5095–5102.

Nakagawa S, Schielzeth H (2013) A general and simple method for obtaining R2 from generalized linear mixed-effects models. Methods Ecol Evol 4:133–142.

Osorio-Forero A, Cardis R, Vantomme G, Guillaume-Gentil A, Katsioudi G, Devenoges C, Fernandez LM, Lüthi A (2021) Noradrenergic circuit control of non-REM sleep substates. Curr Biol 31:5009–5023.e7.

Paxinos G, Watson C (2006) The rat brain in stereotaxic coordinates, Ed 6. Amsterdam: Elsevier.

Pernia-Andrade AJ, Jonas P (2014) Theta-gamma-modulated synaptic currents in hippocampal granule cells in vivo define a mechanism for network oscillations. Neuron 81:140–152.

Perogamvros L, Schwartz S (2012) The roles of the reward system in sleep and dreaming. Neurosci Biobehav Rev 36:1934–1951.

Puentes-Mestril C, Roach J, Niethard N, Zochowski M, Aton SJ (2019) How rhythms of the sleeping brain tune memory and synaptic plasticity. Sleep 42:zsz095.

R Core Team (2021) R: A language and environment for statistical computing. R foundation for statistical computing, Vienna. Available at https://www.R-project.org/.

Rasch B, Born J (2013) About sleep's role in memory. Physiol Rev 93:681–766.

Raven F, Van der Zee EA, Meerlo P, Havekes R (2018) The role of sleep in regulating structural plasticity and synaptic strength: implications for memory and cognitive function. Sleep Med Rev 39:3–11.

Salin PA, Scanziani M, Malenka RC, Nicoll RA (1996) Distinct short-term plasticity at two excitatory synapses in the hippocampus. Proc Natl Acad Sci USA 93:13304–13309.

Schall KP, Kerber J, Dickson CT (2008) Rhythmic constraints on hippocampal processing: state and phase-related fluctuations of synaptic excitability during theta and the slow oscillation. J Neurophysiol 99:888–899.

Seibt J, Frank MG (2019) Primed to sleep: the dynamics of synaptic plasticity across brain states. Front Syst Neurosci 13:2.

Stevens CF, Wang Y (1995) Facilitation and depression at single central synapses. Neuron 14:795–802.

Tononi G, Cirelli C (2014) Sleep and the price of plasticity: from synaptic and cellular homeostasis to memory consolidation and integration. Neuron 81:12–34.

Trouche S, Koren V, Doig NM, Ellender TJ, El-Gaby M, Lopes-Dos-Santos V, Reeve HM, Perestenko PV, Garas FN, Magill PJ, Sharott A, Dupret D (2019) A hippocampus-accumbens tripartite neuronal motif guides appetitive memory in space. Cell 176:1393–1406.e16.

Vyazovskiy VV, Cirelli C, Pfister-Genskow M, Faraguna U, Tononi G (2008) Molecular and electrophysiological evidence for net synaptic potentiation in wake and depression in sleep. Nat Neurosci 11:200–208.

Winson J, Abzug C (1977) Gating of neuronal transmission in the hippocampus: efficacy of transmission varies with behavioral state. Science 196:1223–1225.

Zhang CL, Houbaert X, Lepleux M, Deshors M, Normand E, Gambino F, Herzog E, Humeau Y (2015) The hippocampo-amygdala control of contextual fear expression is affected in a model of intellectual disability. Brain Struct Funct 220:3673–3682.